Helium Atom Scattering Studies of the Structures and Vibrations of the H_2, HD, and D_2 Monolayers on NaCl(001)†

Franziska Traeger* and J. Peter Toennies

Max-Planck-Institut für Strömungsforschung, Bunsenstrasse 10, D-37073 Göttingen, Germany

Received: February 8, 2004; In Final Form: June 15, 2004

The structures and vibrations of monolayers of both normal and para-H_2 as well as of HD and D_2 on single-crystal NaCl(001) surfaces have been studied with high-resolution helium atom scattering at surface temperatures of 8 K. The diffraction patterns of all of these systems are consistent with a (1×1) structure, thereby simplifying the interpretation of the time-of-flight spectra. For p-H_2, a well-resolved dispersionless inelastic peak with $\Delta E = 7.0$ meV can be assigned to vibrations parallel to the surface and is accompanied by slightly anharmonic overtones at $\Delta E = 11.8$ and 17.2 meV. The fundamental adsorbate mode hybridizes at larger wave vectors with the Rayleigh mode of the substrate producing an additional branch at 8.5 meV. For ortho-H_2, the vibrational frequencies are greater by about 1 meV but are otherwise similar. The frequencies for HD and D_2 are largely consistent with the expected mass-induced shifts in the frequencies. There is also some evidence for rotational excitation of the adsorbed HD molecule.

1. Introduction

The first studies of hydrogen molecule−surface interactions were scattering experiments from cleaved alkali halide crystals.[1−3] One of the aims of these pioneering experiments, carried out in the early 1930s by Stern's group in Hamburg, was to confirm de Broglie's hypothesis that atoms and molecules also exhibit wavelike behavior.[4] H_2 and He were chosen because of their light masses and large de Broglie wavelengths and diffraction angles. Subsequently, this field of research remained dormant until about 1980. Despite the recent renaissance of He atom scattering (HAS) from surfaces and its development into a powerful tool for structural and dynamical studies of solid surfaces, it is only since the mid-1970s that a few studies of high-resolution hydrogen molecule scattering from surfaces have been reported.[5−12] Perhaps one of the most interesting phenomena observed is the surprisingly strong dependence of the diffraction probabilities on the nuclear spin states of the hydrogen isotope. Thus, the 1995 predictions of Kroes and Mowrey that ortho-H_2 molecules (with spin $I = 1$ and the rotational states $j = 1, 3, 5, ...$) and p-H_2 ($I = 0$, $j = 0, 2, 4, ...$)[13−15] would have different diffraction intensities in scattering from LiF(001) was subsequently confirmed in our laboratory for the (001) surfaces of LiF, NaCl, KCl and MgO.[16−18]

Other recent studies of H_2 interactions with insulators were focused on H_2 adsorbates on MgO powder with a large surface-to-volume ratio. These were investigated with neutron scattering,[20−23] heat capacity,[21,22,24] and NMR[25] techniques. An even greater number of studies have been carried out for hydrogen adsorbates on exfoliated graphite, see, for example, refs 26−34.

The underlying theory for understanding hydrogen adsorbates has also recently been extended to include the quantum effects required by virtue of the light mass of the adsorbate.[35,36] These and many other studies of hydrogen with surfaces are motivated to a large extent by the simplicity of hydrogen and the possibility of a fundamental theoretical treatment of the system.

The present HAS study of H_2 adsorbed on NaCl(001) is an extension of a recent HAS investigation of the three hydrogen isotopomers on MgO(001).[37] In these experiments, the H_2 molecules are first adsorbed on the single-crystal surface and the external vibrations of the molecules are interrogated by inelastic helium atom scattering. These experiments were made possible by the development of a low temperature (∼8 K) target holder.[37] Not only do they complement the earlier studies of H_2 isotope scattering from the same surface, but they also complement the infrared spectroscopy studies on the external vibrations made by Heidberg and Ewing and their collaborators.[35,36,38−44]

The technique of He atom scattering (HAS) used here has several important advantages over the other major surface scattering techniques of low-energy electron diffraction (LEED) and electron energy loss spectroscopy (EELS). For one because the probe particle is neutral, problems with surface charging are avoided altogether. Moreover, because of the much lower energies of typically 30 meV for He atoms compared to 5−100 eV for electrons, the atoms do not in any way perturb these very weakly bound adsorbate layers. Indeed, these adsorbates are so delicate that even atom beams with slightly higher incident energies of ≥35 meV have been found to stimulate desorption of H_2 films.[17,45] Finally, the problem of the small scattering cross section from H_2 molecules encountered in all studies with electrons is also circumvented.

Perhaps one of the most interesting general results coming from the present work is the large qualitative differences between both the structure and the vibrations of H_2/NaCl compared to the previous HAS study of H_2/MgO.[37] This demonstrates the remarkable and perhaps surprising sensitivity of H_2 quantum adsorbates to small differences in substrate properties such as the lattice constant or the potential corrugation.

This article is organized as follows: First, the experimental method is briefly described in section 2. In the next section, the results from helium diffraction and inelastic scattering

† Part of the special issue "Gerhard Ertl Festschrift".

* To whom correspondence should be addressed. Present address: IWV-1, Forschungszentrum Jülich, 52425 Jülich, Germany. E-mail: f.traeger@fz-juelich.de.

10.1021/jp049430s CCC: $27.50
Published on Web 08/04/2004

TABLE 1: Some Physical Properties of NaCl

property	symbol	value	ref
lattice constant	a	5.64 Å	51
density	ρ	2.165 g/cm^3	52
melting point	T_m	1073.8 K	51
bulk Debye temp	Θ_D (bulk)	321.5 K	51
surface Debye temp	Θ_D (surface)	240−250	53, 54
HAS corrugation ampl	ξ	0.34 Å	55
surface lattice dynamics calc.	−	see Ref.	56, 57
surface dispersion curve (HAS)	−	see Ref.	58−60

TABLE 2: Ground Rotational States and Lowest Rotational Transition Energies of the Hydrogen Isotopomers in Their Vibrational Ground State[66]

isotopomer	ground rotational state	proportion in gas phase (%)	rotational transition	ΔE_{rot} (meV)
ortho-H_2	$j = 1$	75	$1 \rightarrow 3$	72.77
para-H_2	$j = 0$	25	$0 \rightarrow 2$	43.93
HD	$j = 0$	no spin isomerism	$0 \rightarrow 1$	11.06
ortho-D_2	$j = 0$	66.7	$0 \rightarrow 2$	22.20
para-D_2	$j = 1$	33.3	$1 \rightarrow 3$	36.89

measurements are presented. The adsorbate structure and the assignment of the external vibrations are subsequently discussed in section 4. After a short outlook on the possibility of superfluid 2D-layers in section 5, the main conclusions are summarized in section 6.

2. Experimental Section

Because both the HAS technique for elastic and inelastic surface studies and the present apparatus[46−48] are well documented, the instrument description will be brief with only additional relevant details added. A highly collimated, nearly monoenergetic He atom beam is formed in a free jet expansion through a 10-μm-diameter thin walled orifice from a source with stagnation temperatures (T_0) that can be varied from 50 to 340 K and source pressures of $P_0 = 10-450$ bar. The atom beam has velocities between $v = 700$ m/s ($k_i = 4.4$ Å^{-1}) at $T_0 = 50$ K and $v = 2000$ m/s ($k_i = 12.4$ Å^{-1}) at $T_0 = 340$ K corresponding to kinetic energies (E_i) between 10 and 80 meV. The fwhm of the beam energy is about 2% over this energy range. To avoid collision-induced desorption of the molecular adsorbates in the present experiments, incident energies below about 35 meV are used. After scattering from the target, the atoms are detected by an electron bombardment ionizer mass spectrometer located at the end of a flight tube about 143 cm from the surface sample. The angle between the incident and the scattered beam is fixed at $\theta_i + \theta_f = 90°$, where θ_i and θ_f are the incident and scattering angles measured with respect to the surface normal. Different scattering conditions were obtained by rotating the azimuthally aligned single crystal around an axis normal to the scattering plane, thereby simultaneously changing the incident and final scattering angles θ_i and θ_f, respectively.

Cleavage in situ in a vacuum of the $10 \times 10 \times 10$ mm^3 NaCl crystals as in most of the recent HAS experiments was impaired by the necessity to enclose the target crystal by a cryocooled radiation shield. Instead, the crystals were cleaved ex situ under argon atmosphere and firmly clamped into a recess of the copper sample holder, around which a copper cylinder with a 5-mm slit for the incident and outgoing He beam was mounted.[49] The cryostat with the sample was then transferred as quickly as possible into the scattering chamber, which was evacuated to 10^{-4} mbar within 60−90 min after cleavage. The continuous-flow liquid-helium-cooled manipulator is described in more detail in ref 37. The lowest surface temperature reached in these experiments was 8 K, measured with a silicon diode[50] attached to the sample holder close to the crystal. The target chamber was baked for 24−30 h at 200 °C, but the manipulator only reached a temperature of about 130 °C. A base pressure of 8.5×10^{-11}mbar was achieved. Table 1 lists some important physical properties of NaCl crystals. The surface phonon dispersion curves have been extensively studied using HAS (for example, refs 58−60) as well as in several calculations (e.g., refs 56 and 57).

The quality of the surface was checked in situ by comparing He diffraction intensities and specular peak widths in the angular distributions with those of previous studies.[61] Three of the four cleaves performed in air resulted in good surfaces with sharp diffraction peaks, indicating domain sizes comparable to those obtained earlier[61] with vacuum-cleaved surfaces. The signal, however, was about a factor of 3 lower, and the relative intensity of the diffuse elastic peak in the time-of-flight spectra was considerably larger than for surfaces cleaved under UHV. Both differences can be attributed to a larger number of randomly distributed defects created in the cleaving process under atmospheric pressure.

In most experiments, the hydrogen layer was prepared by backfilling the gas through a leak valve directly into the chamber, where the sample crystal was held at about 8 K. Because the surface temperature was not low enough to stabilize the adsorbed layer without a hydrogen background pressure all measurements, except those shown in Figure 16 below, were carried out under continuous gas exposure. The steady-state pressures were sufficiently low ($<10^{-6}$ mbar) that the He atom beam was not noticeably attenuated. The increase in the background gas pressure was further reduced in some of the experiments by about a factor of 5 by mounting a Teflon tube on the gas valve which ended about 10 mm in front of the crystal and therefore allowed a more direct dosage. The exposures are given in units of Langmuirs ($1\ L = 1 \times 10^{-6}$ Torr·s). However, because the sticking coefficient is less than 1 and the adsorption is reversible at 8 K, an exposure of 1 L corresponds to a coverage of less than a monolayer.

Normal H_2 (n-H_2: 75% ortho-, 25% para-H_2) with a purity of 99.999%,[62] D_2 with a purity of 99.7%,[62] and HD with a purity of 97% (1.2% D_2, 1.8% H_2)[63] were used without additional treatment. Para-H_2 (p-H_2) with less than 4% residual ortho-H_2 was prepared from liquid hydrogen using an iron oxide/chromium oxide catalyst.[64,65] Because impurities such as CO or water molecules adsorb irreversibly and accumulate on the surface at low surface temperatures, great care was taken in baking and purging the adsorbate gas line, which was evacuated between experiments with a turbomolecular pump. At 8 K, all of the molecules studied are in their lowest rotational states (Table 2).

The angular distributions are displayed as a function of incident angle. They can be converted to parallel momentum transfer according to the relation

$$\Delta K = k_i(\sin \theta_f - \sin \theta_i) \quad (1)$$

For the inelastic time-of-flight (TOF) measurements, the beam was chopped at 500 Hz by a rotating disk with two oppositely positioned V-shaped slits, which led to narrow pulses of 12-μs half-width. For a single TOF spectrum the signal was usually integrated over 1×10^6 or 2×10^6 cycles corresponding to 33 or 66 min, respectively. After subtraction of a linear background, the time-of-flight spectra are converted to an energy loss scale (ΔE) and the measured intensity is multiplied by the Jacobian

$$\left|\frac{dt_{TD}}{d\Delta E}\right| = \frac{t_{TD}^3}{mL_{TD}^2} \quad (2)$$

where m is the mass of the He atom and L_{TD} and t_{TD} are the distance and flight time, respectively, between the target crystal and detector. The corresponding momentum transfers, ΔK, are then obtained from the "scan curve" expression[67]

$$\frac{\Delta K}{K_i} = -1 + \sqrt{\left(\frac{\Delta E}{E_i} + 1\right)\frac{\sin^2\theta_f}{\sin^2\theta_i}} \quad (3)$$

where E_i is the incident energy and K_i is the component of the incident wave vector parallel to the surface ($K_i = k_i \sin\theta_i$). To account for Umklapp processes the wave vector transfers are reduced using the expression $Q = |\Delta K| - |G_{mn}|$, where G_{mn} is the reciprocal lattice vector of the nearest diffraction peak, and then folded into the first Brillouin zone. An entire dispersion curve up to the Brillouin zone boundary is obtained from a series of time-of-flight spectra measured at incident angles between the first-order diffraction peaks in steps of either 0.5° or 1°. Up to about 20 time-of-flight spectra were measured at different angles of incidence for each crystal direction and for the [110] direction at two incident beam energies.

3. Results

3.1. Adsorption Curves. To follow the adsorption of H_2, an "adsorption curve" was recorded by monitoring the specularly scattered He signal as a function of time after the initiation of gas exposure. Four typical adsorption curves for n-H_2 on NaCl are shown in Figure 1. Curves a−c in Figure 1 were measured along the [110] crystal directions at incident energies of 10, 15, and 26 meV, respectively, whereas curve d was measured along the [100] direction at an incident energy of 26 meV. In each case, the specular intensity first decreases because initially the adsorbed molecules act as randomly distributed point defects with large scattering cross sections.[68] Then, with increasing coverage, the intensity passes through a minimum and subsequently increases as small ordered islands, which finally coalesce, are formed. After an exposure of between 2 and 3 L, the intensity levels off, indicating steady-state conditions corresponding to the formation of a saturated layer, which is assigned to a monolayer. This growth behavior is different from that observed for CO_2/NaCl(001),[69] where large islands are formed at the outset. The final steady-state specular signal depends on the defect density of the layer, its Debye temperature and the extent to which the specular peak is depleted by the Bragg diffraction peak intensity.

The accumulation of an appreciable concentration of impurities within the adsorbate layer could be ruled out by measuring the specular intensity during thermal desorption of the layer after each experiment. Because impurities such as N_2, CO, and H_2O are much more strongly bound than H_2, they can be identified, if present, by a further increase in He intensity at desorption temperatures above the 18 K at which hydrogen, even under continuous gas dosage, is desorbed.

The somewhat different surface temperatures and n-H_2 gas pressures used in the four experiments shown in Figure 1 have no significant influence on the overall form of the adsorption curves and only a slight influence on the exposures needed to form a stable layer. The adsorption curves for the hydrogen isotopomers HD and D_2 as well as for p-H_2, which are not shown here, all have similar shapes. Quite remarkable is the finding that, after completion of the monolayer, the scattered He intensity is relatively large and sometimes even greater than for the clean surface (see curves b and d). This, very likely, reflects the low defect density and the different corrugation of the film (see Figure 4 below). For a particular beam energy, the corrugation determines the fraction of the intensity transferred out of the specular peak into the diffraction channels.

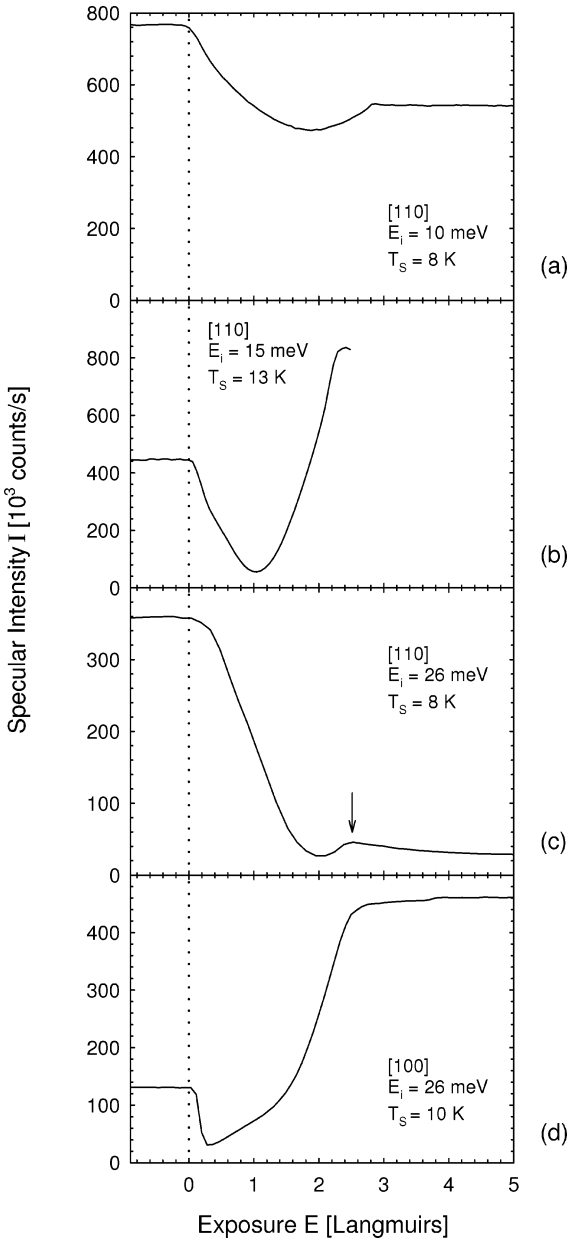

Figure 1. Measurements of the specular intensity as a function of the exposure of the NaCl(001) surface to n-H_2 (adsorption curves) for the different crystal azimuths, incident beam energies, and surface temperatures listed in each panel. The H_2 gas pressures were (a,b) 4×10^{-8}, (c) 9×10^{-8}, and (d) 1×10^{-7} mbar. The leveling off of the curves beyond exposures of about 2−3 L is interpreted as indicating the formation of a monolayer. The arrow in panel c indicates a small maximum possibly due to ortho−para exchange.

In some of the n-H_2 adsorption curves as well as in some of the desorption curves (not shown), a small peak similar to the one indicated by an arrow in panel c of Figure 1 was found close to monolayer exposure. The fact that this peak was seen in desorption curves of n-H_2 only after a prolonged gas exposure, of 10−20 min or more, suggests that the molecules might have first diffused, before locking into more energetic sites to produce a more ordered surface. Because this bump is not observed for a pure p-H_2 layer, replacement processes favoring ortho-H_2 from

the ambient gas over initially adsorbed para-H_2 could also explain the delayed formation of an ordered layer. For this adsorbate system, such replacement processes have indeed been reported by Heidberg et al.[35] The observed slow decrease in the intensity of the small peak at exposures greater than 2.5 L could be due to the slow adsorption of impurities from the residual gas background or to a slight thermally induced misalignment of the crystal.

The adsorption energies, E_{ads}, were estimated using the equality of the chemical potentials μ for the gas and 2D monolayer, which is the condition for equilibrium between gas phase and 2D adsorbed phase.[70] The equality of μ can be written as:

$$k_B T \ln(n_3 \lambda^3) = E_{ads} + k_B T \ln(n_2 \lambda^2) \quad (4)$$

where T is the surface temperature, n_2 is the density of the adsorbed (1 × 1) hydrogen film, $n_3 = p/k_B T$ is the gas-phase density; and $\lambda = \sqrt{2\pi\hbar^2/mk_B T}$ with m being the mass of the hydrogen isotopomer and k_B the Boltzmann constant. From the measured equilibrium gas pressures and the surface temperatures at several adsorption−desorption cycles, adsorption energies of ~40 meV were estimated for n-H_2 as well as for HD, compared to 37 meV for p-H_2. The uncertainty in the absolute values is at least ±5 meV, but the same relative trends were present in all of the measurements. These results will be compared with other experiments and theory in section 4.3.

3.2. Angular Distributions. More direct information regarding the adsorbate structure comes from the angular distributions, which provide the positions of the Bragg peaks in reciprocal space and the symmetry of the surface unit cell. In Figure 2, angular distributions along the [100] direction for the clean surface (left) and a monolayer of n-H_2 (right) are shown, measured with different incident wave vectors between 4.55 and 8.13 Å^{-1} corresponding to incident energies between 10.8 and 34.5 meV. As already expected from the adsorption curves in Figure 1, the intensities of the monolayer angular distributions are comparable to those for the clean surface, and these relative intensities are considerably higher than for other molecular adsorbates.[69,71−73] All of the monolayer diffraction peaks are at precisely the same positions as and of comparable widths to those of the bare NaCl substrate. Also, along the other azimuthal direction, [110] (Figure 3), no additional peaks were found.[75] Both observations are in accord with a well-ordered (1 × 1) monolayer structure, as proposed in the literature,[35,36] although diffraction measurements along only two crystal directions are, in fact, not sufficient for a unique determination. However, a structure with different adsorption sites at different heights above the surface plane as proposed by Grunwald and Ewing,[44] which is also consistent with the diffraction patterns, is not consistent with the observation of only a single jump in the adsorption curves. The different conclusions of Grunwald and Ewing and the present experiment might be due to differences in the experimental conditions and will be discussed in more detail in section 4.

Despite the close similarity of the adsorbate and clean substrate diffraction patterns, there are two important differences. For one, the relative intensities of the diffraction peaks change with incident wave vector in a different way for the monolayer than for the clean surface. This indicates that the monolayer has a considerably different corrugation profile than the clean NaCl substrate. Moreover, the more pronounced decrease of the adsorbate peak intensities with increasing incident wave vector compared to the clean surface indicates a larger Debye−

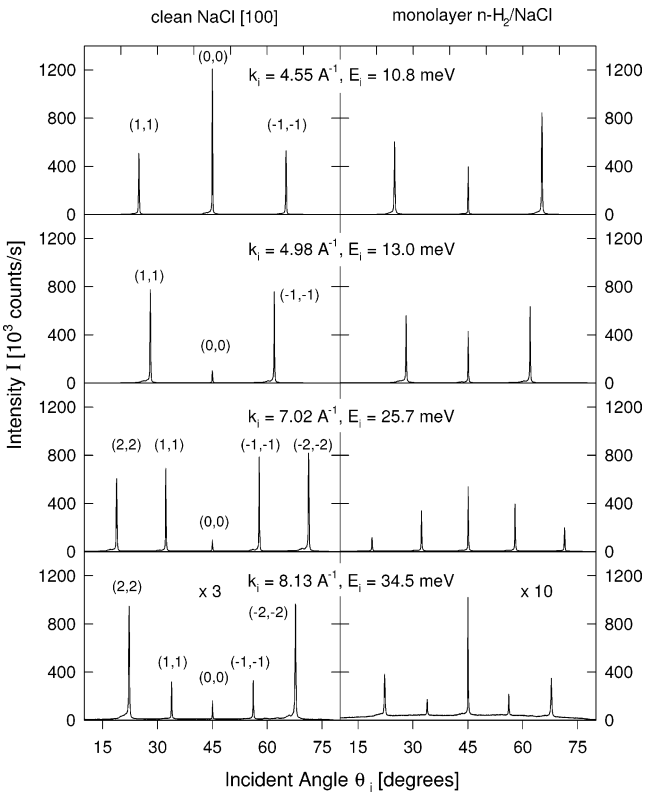

Figure 2. Angular distributions of helium atoms diffracted along the [100] direction from the clean NaCl(001) surface (left column) with measurements from a monolayer n-H_2 on NaCl(001) (right column) for four different incident wave vectors of the He beam between 4.55 and 8.13 Å^{-1} (top to bottom). The expected decrease in the angular spacing of the peaks with increasing wave vector is clearly apparent. The monolayer was prepared and maintained on the surface under continuous dosage of (1 × 10^{-7})−(2 × 10^{-6}) mbar of H_2 at surface temperatures between 10 and 13 K. Because no additional superstructure peaks are visible, the intensities clearly indicate a well ordered (1 × 1) adsorbate layer.

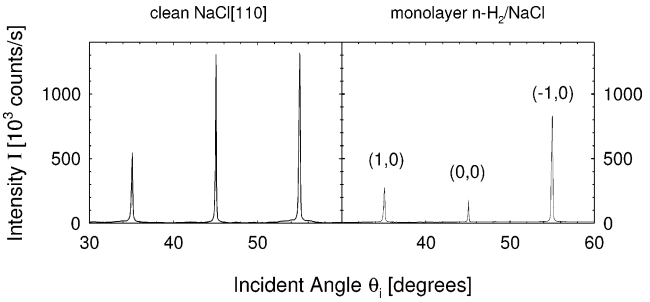

Figure 3. Angular distributions of the clean surface (left) and an adsorbate at 8 K under 2.2 × 10^{-7} mbar of n-H_2 (right) measured along the [110] direction with an incident wave vector of 6.5 Å^{-1} (E_i = 22.1 meV). The differences in the (1,0) and (−1,0) Bragg peak intensities are due to a slight misalignment of the crystal.

Waller attenuation. This implies that the adsorbate vibrations are softer than the substrate vibrations as indeed observed in the time-of-flight spectra discussed in section 3.3.

Angular distributions measured prior to monolayer completion provide important information on the layer growth mechanism. As shown in Figure 4, a closer examination of the adsorbate specular peak during the initial stages of adsorption reveals a factor of 2 greater width compared to the bare surface. Upon completion of the layer, the width decreases again to the initial width of the clean surface. At present, this broadening cannot be explained unambiguously. Possible interpretations include an initial clustering of the adsorbed molecules or a large initial

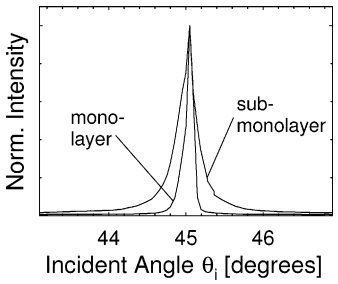

Figure 4. Specular peak shape at submonolayer coverage compared to the same peak measured for a complete monolayer produced under a n-H_2 gas pressure of 1.7×10^{-8} mbar at 8 K and at $E_i = 15$ meV.

defect density, both of which will disappear upon further adsorption and ordering of the layer. In the case of clustering the fwhm peak width $\delta\Delta K$ would reflect the island diameter a according to $\delta\Delta K = 2\pi/a$. If the molecules initially adsorb singly and act as randomly distributed defects, the diffraction signal from the clean surface areas will be reduced. The specular peak will appear to be broadened due to scattering from the single adsorbed molecules.[74] Finally, it is noted that both clustering and ordering of the layer at higher coverages imply a high mobility of the adsorbate despite the low surface temperatures.

3.3. Time-of-Flight Spectra. To investigate the external vibrations of the hydrogen monolayer, time-of-flight spectra were recorded at $E_i = 26.5$ meV ($k_i = 7.1$ Å^{-1}) over a range of incident angles (θ_i) between 38° and 48−52°. At this incident energy, the corresponding scan curves (see eq 3) extend over at least three Brillouin zones, and phonons with energies up to about 20 meV can be created while collision-induced desorption[45] as well as multiphonon excitations are largely avoided. At higher incident energies, these processes will dominate over the single phonon signals, as discussed earlier.

Figure 5 displays a series of time-of-flight spectra (converted to an energy scale) measured along the [110] direction from a monolayer of p-H_2. In these and all other TOF spectra presented in this paper, the background was subtracted. With the exception of the D_2 layers, the background signal was typically 20−80 counts/s. The layer in Figure 5 was stabilized under adsorption−desorption equilibrium at 1×10^{-7} mbar of p-H_2 and a surface temperature of 8 K. The peak at zero energy transfer, which is mostly due to diffuse *elastic* scattering, is, in contrast to many other adsorbate systems studied in the past,[76] relatively small compared to the phonon peaks. This confirms the excellent ordering of the layer and the small number of defects as deduced from the narrow width of the specular peak (see Figure 4). A broad intensity maximum at specular incidence is expected for elastic scattering from defects. The origin of the diffuse elastic scattering will be discussed in more detail in section 4.2.

At the low surface temperature of 8 K, all external vibrations are expected to be in their ground states. For this reason, no additional features were found at positive (annihilation) energy transfers, also at energy transfers beyond +5 meV, not shown in Figure 5. Thus, the *inelastic* phonon peaks are dominated by negative energy transfers, corresponding to creation events. On the creation side, three groups of peaks can be distinguished: (i) a single main peak between −6 and −8 meV and at least two additional peaks with $|\Delta E| \leq 9$ meV, all of which depend on the incident scattering angle; (ii) two distinct sharp peaks at about −12 and −17 meV and between these a broad maximum at large angles θ_i and up to four small peaks at small angles; and finally (iii) some weak structures at higher energy transfers. These data and a few additional spectra are displayed in Figure

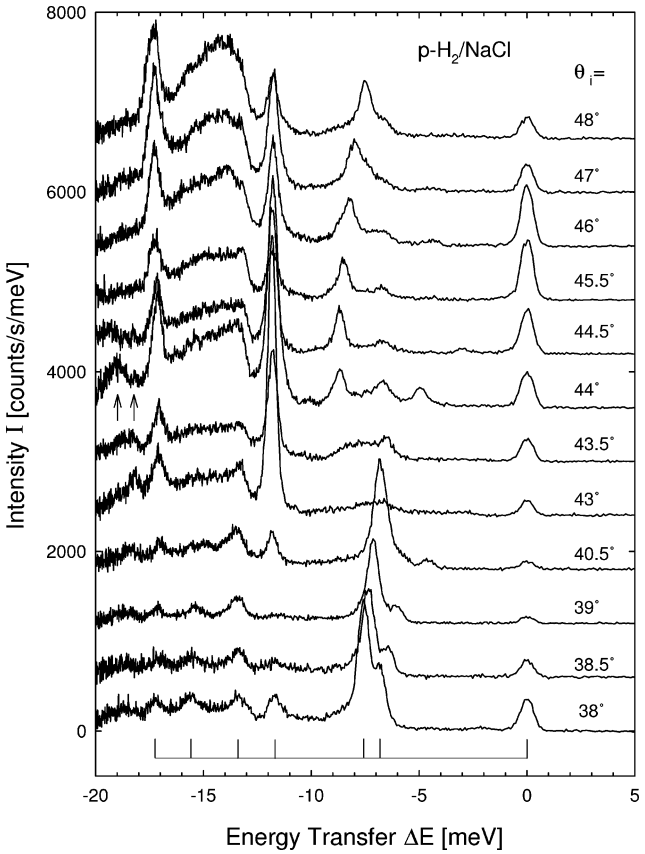

Figure 5. Series of time-of-flight spectra from a monolayer of p-H_2 on NaCl(001) along the [110] direction between incident angles of θ_i = 38° and 48°. All spectra were measured under 1×10^{-7} mbar of p-H_2 gas pressure at a surface temperature of 8 K and with an incident beam energy of 26.5 meV. For clarity the curves are offset vertically by 600 (counts/s)/meV with respect to each other. The arrows indicate peaks at larger energy transfers, which might be S modes as discussed in section 4.2.

6a in an extended-zone plot and in Figure 6b in the corresponding reduced-zone plot. Again, the same groups of phonon peaks can be distinguished. Of these, only a few points can be assigned to the NaCl Rayleigh mode. In the outer part of the Brillouin zone, a new mode is now seen more clearly at 8.5 meV after a crossing of the 7 meV mode with the NaCl Rayleigh mode. In panel a, two typical scan curves for the incident angles of 38° and 47° are also shown, of which the first corresponds to the bottom spectrum in Figure 5. The assignment of these modes is discussed in section 4.2.

Surprisingly, the TOF spectra of a submonolayer of p-H_2 on NaCl (not shown) exhibit nearly the same phonon features as the full layer. As discussed in section 3.2, the specular-peak broadening during adsorption prior to completion of the first layer can be explained by scattering either from monolayer clusters or from randomly distributed single molecules. Both possibilities can also explain the similarity in the phonon features. If single molecules are involved, the submonolayer TOF spectra indicate that the isolated molecules have vibrational frequencies identical to those of the full layer. This would imply only a negligible lateral coupling between the adsorbate molecules in the case of the full layer, as found for monolayers of rare gases on Pt(111).[77] Indeed, this is also compatible with the small dispersion of the adsorbate modes seen in Figure 6.

Figure 7 shows a series similar to that in Figure 5, which was measured under comparable beam conditions and surface temperatures for a n-H_2 monolayer at P(n-H_2) = 9×10^{-8} mbar. In interpreting these results, it should be noted that, at the

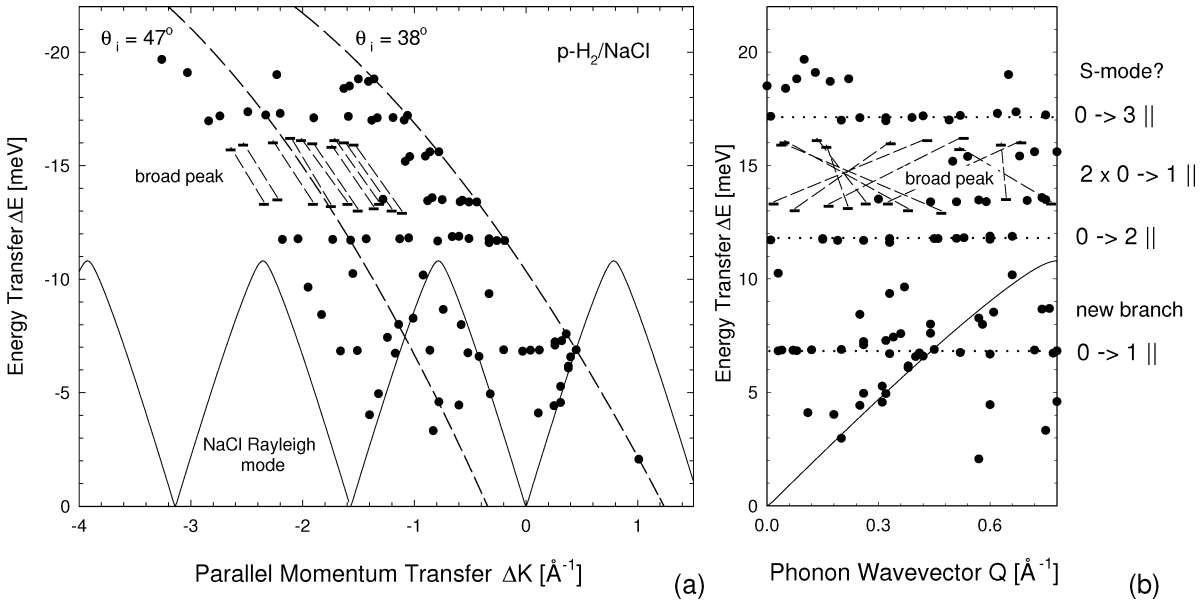

Figure 6. (a) Extended-zone plot and (b) folded dispersion diagram of the external vibrations of a monolayer of p-H_2 on NaCl(001) along the [110] azimuthal direction. The experimental conditions can be found in the Figure 5 caption. The dashed lines represent scan curves for the spectra measured at $\theta_i = 38°$ and 47° shown in Figure 5. Sharp peaks are indicated with filled circles, whereas the broad energy transfers observed at larger negative parallel momentum transfers are indicated by the energy ranges connected by dashed lines. The assignments of the modes indicated in b on the right-hand side are discussed in section 4.

surface, the ortho/para composition might differ from the 75% ortho- and 25% para-H_2 gas-phase composition, because the sticking probabilities and the adsorption energies are different for the different spin modifications.[35,36] Qualitatively, the HAS time-of-flight spectra from the n-H_2 monolayer are similar to those from the p-H_2 layer. As for p-H_2, one group of inelastic peaks of varying intensity is located between −4 and −9 meV; in addition, several somewhat sharper peaks are found between −12 and −18 meV, and at higher incident angles, a broad intermediate maximum can be seen. All of these peaks, however, are broader than those for p-H_2, which can be attributed to differences in the excitation energies of the adsorbed p-H_2 and o-H_2 molecules. Of a total of 11 deconvolutions at different incident angles (spectra in Figure 7 and additional data), two are shown in Figure 8 for TOF spectra measured at incident angles of 42° and 44.5° at the same incident beam energy of 26.5 meV. The broad energy transfer peaks of n-H_2 were fitted by assuming that the p-H_2 component was already known from the pure p-H_2 spectrum measured under identical conditions, so that the remaining intensity can be assigned to the corresponding vibrational transitions of o-H_2. The extracted o-H_2 vibrational energies were averaged over all deconvolutions to minimize the uncertainty of the single fits. This procedure requires that the o-H_2 vibrations do not show any dispersion, which is justified, because also in the spectra of pure p-H_2, no dispersion was found. In this way, average phonon losses at −7.7, −13.2 (both ±0.5), and −15.3 meV are attributed to o-H_2, where the latter peak appears to be an overtone of the 7.7 meV mode. Because of the congestion, the exact location of the o-H_2 peak at −15.3 meV is less certain than those of the −7.7 and −13.2 meV peaks.

In the same way as for the p-H_2 adsorbate, the measured energy loss data for the monolayer of n-H_2 are compiled in Figure 9 in unfolded- and reduced-zone plots. For the broad peaks, only their energy ranges are plotted as horizontal dashes that connect the two sides of the unresolved broad peaks in each spectrum. As in the case of p-H_2, at lower parallel momentum transfers, a few points lie on the substrate Rayleigh dispersion curve.

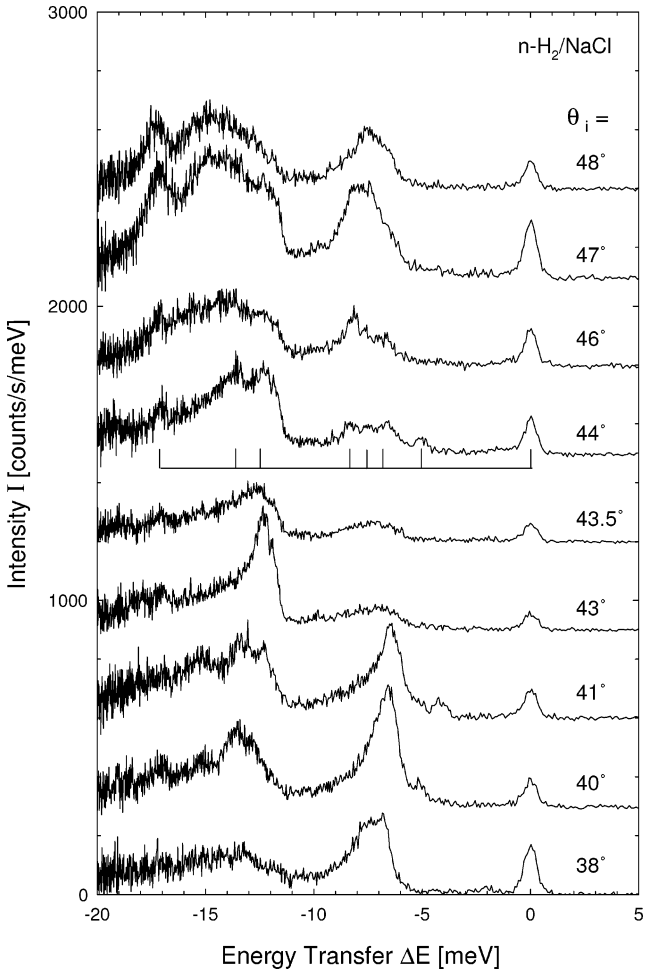

Figure 7. Series of time-of-flight spectra of a monolayer of n-H_2 on NaCl(001) along the [110] direction between incident angles of $\theta_i =$ 38° and 48°. The spectra were measured under 9×10^{-8} mbar of n-H_2 gas pressure at a surface temperature of 8 K and with an incident beam energy of 26.5 meV. For clarity, the curves are offset vertically by 300 (counts/s)/meV with respect to each other.

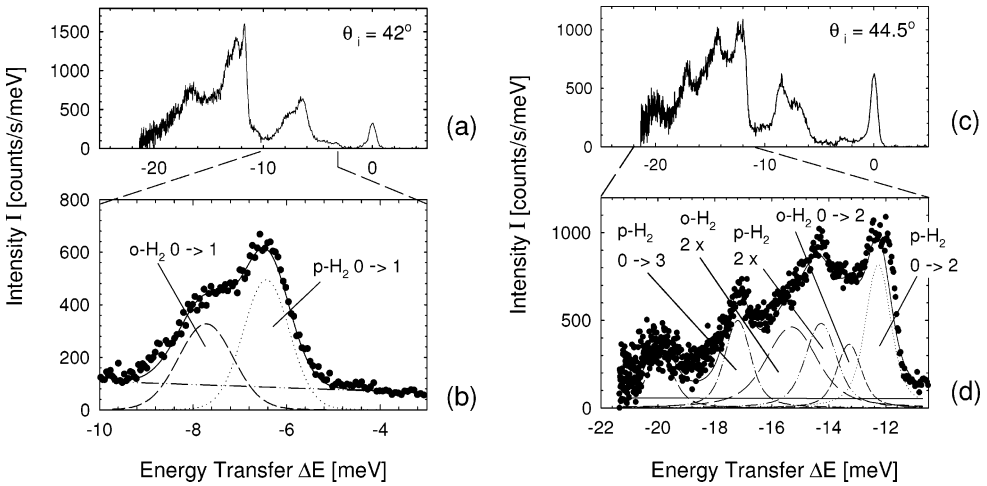

Figure 8. Deconvolution of TOF spectra for a n-H_2 monolayer on NaCl(001) measured at the incident angles of (a) $\theta_i = 42°$ and (c) 44.5° and an incident beam energy of 26.5 meV along the [110] azimuth. For the spectrum in a, the range of energy transfers from −4 to −10 meV is deconvoluted as shown in b and the range from −12 to −20 meV is deconvoluted as shown in d. The mode assignments are discussed in section 4: $0 \rightarrow 1$ denotes the fundamental vibration, $0 \rightarrow 2$, 3 denotes overtones. From deconvolutions of this kind, the fundamental at 7.7 meV and at least one overtone at 13.2 meV can be assigned to o-H_2 with an error of about ±0.5 meV.

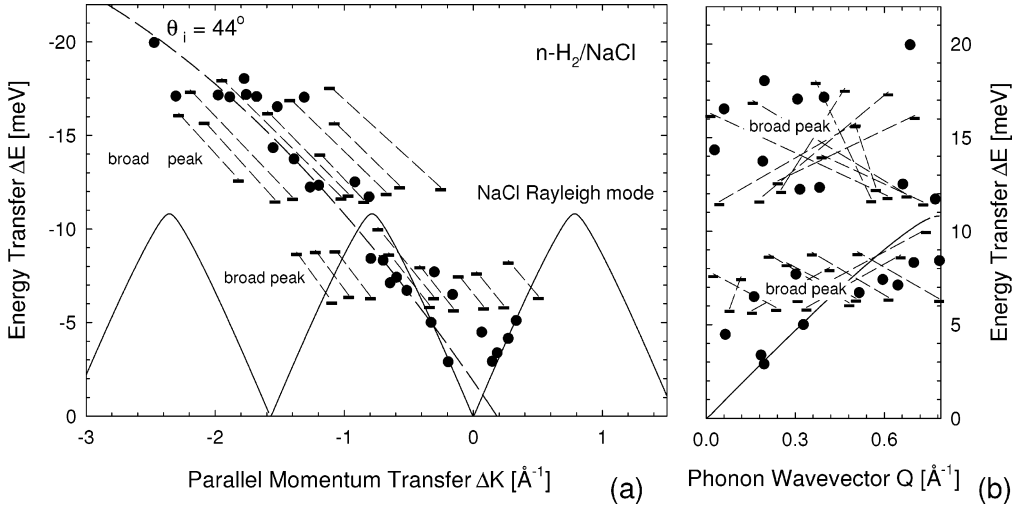

Figure 9. (a) Extended-zone plot and (b) folded dispersion diagram (right) of the external vibrations of a layer n-H_2/NaCl(001) along the [110] azimuth. Parts of the spectra correspond to those shown in Figure 7. The dashed line represents the scan curve for the spectrum at $\theta_i = 44°$ shown in Figure 7. Sharp peaks are indicated with filled circles, whereas for the broad energy transfer peaks, the ranges are indicated by long-dashed connecting lines.

For further comparison, a layer of HD was also studied. The heteronuclear HD molecule does not show ortho-para isomerism (see Table 2), and therefore, all molecules can relax to the $j = 0$ rotational state at these low temperatures. Thus, the HD results can be compared with those of p-H_2, if the isotope shift due to the higher molecular mass, which is given by ($\nu_1/\nu_2 = \sqrt{m_2/m_1}$) for a harmonic oscillator with mass m, is taken into account. Conversely, the isotope shift can be used to confirm the mode assignments.

Because the adsorption curves and angular distributions of HD layers have nearly the same intensities and shapes as those of n-H_2 and p-H_2, they are not shown here. The close similarity indicates that the symmetry of the surface unit cell and therefore the structures as well as the corrugation are the same as for H_2. Figure 10 shows a series of TOF spectra for a HD layer under 1×10^{-7} mbar and at a surface temperature of 8 K. On the phonon-creation side on the left of the diffuse elastic peak, six or more energy transfer peaks are observed between −5 and −20 meV. None is as broad as those found in the n-H_2 spectra, which strengthens the assumption that the n-H_2 peaks do indeed consist of two or more superimposed peaks. Figure 11 shows the usual compilation of the data in unfolded- and folded-zone schemes.

The heavy isotopomer D_2 completes the experiments on the different hydrogen isotopomers and supports the observations already presented. Because 66.7% of the D_2 molecules are expected to be in the $j = 0$ state (see Table 2), the D_2 TOF spectra, after correction for the different mass, should be rather similar to those for p-H_2 and HD. The D_2 TOF spectra are, however, noisier, as the D_2 gas from the target chamber has the same mass as the scattered He atoms and, therefore, gas effusing from the target chamber makes a significant contribution to the background count rate of the mass spectrometer detector. The background is 3−4 times higher than in the H_2 spectra, and the signal is at least a factor of 2 lower, as can be seen in Figure 12a. As in the other TOF spectra, the background intensity, which in this case was about 125−180 counts/s, was subtracted from the spectra shown in Figure 12a, so that its effect is only seen in the greater noise. The measured energy transfers lie at about −5.5, −10.0, and −12.0 meV as well as

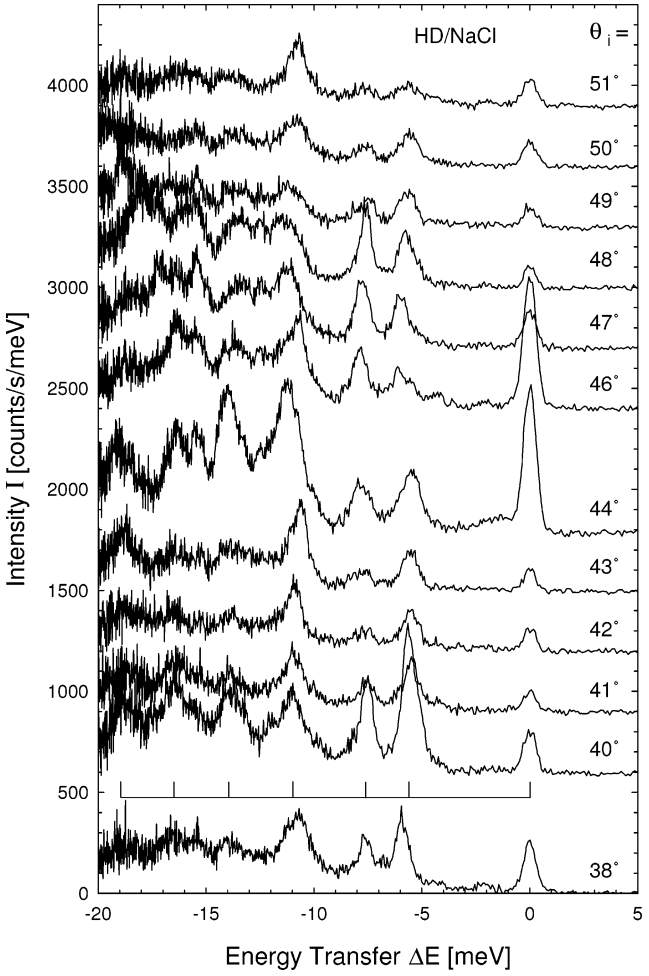

Figure 10. Series of time-of-flight spectra of a monolayer of HD on NaCl(001) along the [110] azimuthal direction between incident angles of $\theta_i = 38°$ and 51°. All spectra were measured under 1×10^{-7} mbar of HD gas pressure at a surface temperature of 8 K and with an incident beam energy of 26.4 meV. For clarity, the curves are offset vertically by 300 (counts/s)/meV per degree of incident angle.

a broad peak at −17.5 meV (Figure 12b). The narrow width of the peak at −5.5 meV suggests that additional unresolved peaks probably do not contribute significantly, implying possibly a suppression of the expected 33.3% $j = 1$ p-D_2 concentration.

Figure 13 provides an overview summary of the TOF spectra of the NaCl(001) surface without and with monolayers of n-H_2, p-H_2, HD, and D_2 all at an incident angle of 44° and a beam energy of 26.5 meV. The spectra are taken from the previous figures where the corresponding gas pressure conditions can be found. This comparison again emphasizes that the contributions from the NaCl substrate phonons to the adsorbate spectra are surprisingly small and that the inelastic signal for all adsorbates is large compared to the diffuse elastic peak. Also, the larger n-H_2 line widths, which presumably are due to unresolved contributions from the two spin modifications, are clearly apparent.

The TOF spectra of H_2 measured along the [100] azimuthal direction show the same energy losses around 8 and 13 meV but with lower intensity,[78] and therefore, they are concealed more by the statistical fluctations of the background. The lower intensity might be interpreted as an indication that the vibrations parallel to the surface are polarized along the [110] direction.

4. Discussion

4.1. Assignment of the Adsorbate Structure. For the structure of the saturated H_2 layer on NaCl(001), Heidberg et al.[35] and Grunwald and Ewing[44] each proposed slightly different models. Whereas the former authors based their model on potential energy calculations and infrared spectroscopy, the latter took account only of the results from infrared spectroscopy. Neither of the two experiments provides any information on the periodic structure and symmetry of the layer.

Heidberg et al. proposed a (1×1) structure with molecules in both the $j = 0$ and $j = 1$, $m_j = \pm 1$ states above Na^+ cation sites. According to the calculations of Heidberg et al.[35] the adsorption energies for an isolated adsorbed H_2 molecule in the $j = 1$, $m_j = \pm 1$ state above the cation is 35.2 meV and decreases to 28.2 meV for the $j = 0$ state. For a molecule in the $j = 1$, $m_j = 0$ state above a Cl^- anion, although more polarizable, it is only 18.1 meV.

Thus, in the experiment by Heidberg et al. at surface temperatures of 9−10 K molecules in the $j = 1$, $m_j = 0$ state are not found, because of their considerably lower adsorption energies. The simultaneous adsorption onto neighboring cation and anion sites is ruled out not only on the basis of the different binding energies, but also on steric grounds. The distance between the cation and anion sites of 2.82 Å is much smaller

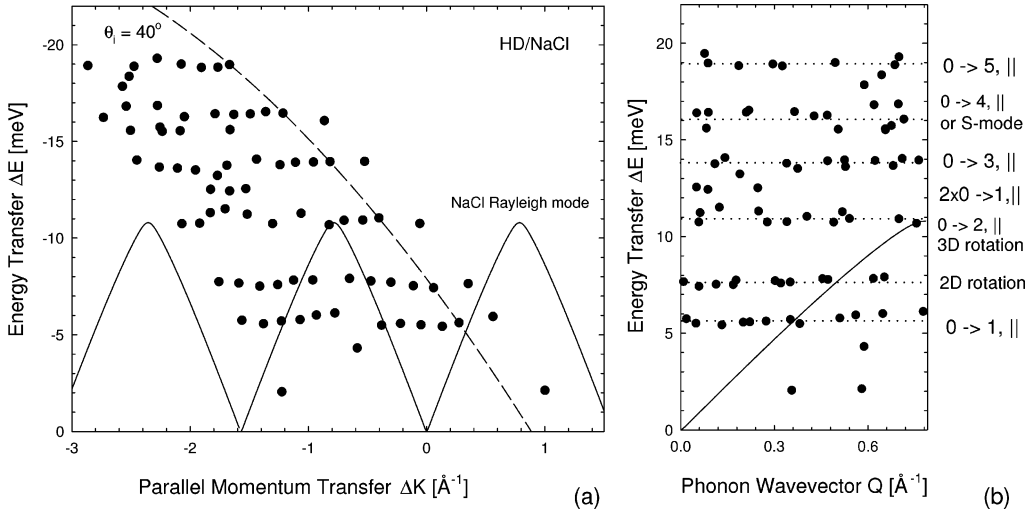

Figure 11. (a) Extended-zone plot and (b) folded dispersion diagram of the external vibrations of a layer HD/NaCl(001) along [110] corresponding to the TOF spectra in Figure 10. The dashed line represents the scan curve for the spectrum at $\theta_i = 40°$ shown in Figure 10. The assignments of the modes on the right-hand side are discussed in section 4. The horizontal dotted lines in the reduced-zone plot are guides to the eye only.

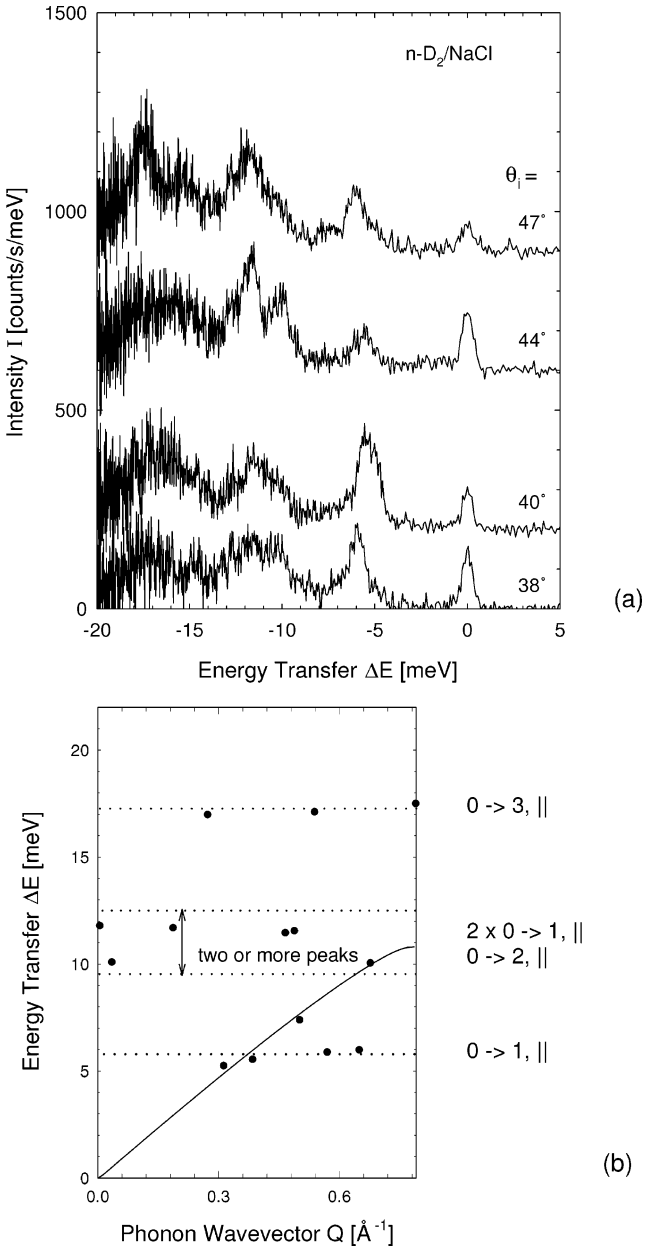

Figure 12. (a) Time-of-flight spectra of a monolayer of n-D_2 on NaCl along the [110] azimuth for the incident angles of $\theta_i = 38°$, 40°, 44°, and 47°. The spectra were measured under $(2-3) \times 10^{-8}$ mbar partial pressure at a surface temperature of 8 K and with an incident beam energy of 26.5 meV. For clarity, the curves are vertically offset by 100 (counts/s)/meV per degree with respect to each other. (b) Results shown in a reduced-zone plot. The assignments of the modes are discussed in section 4.

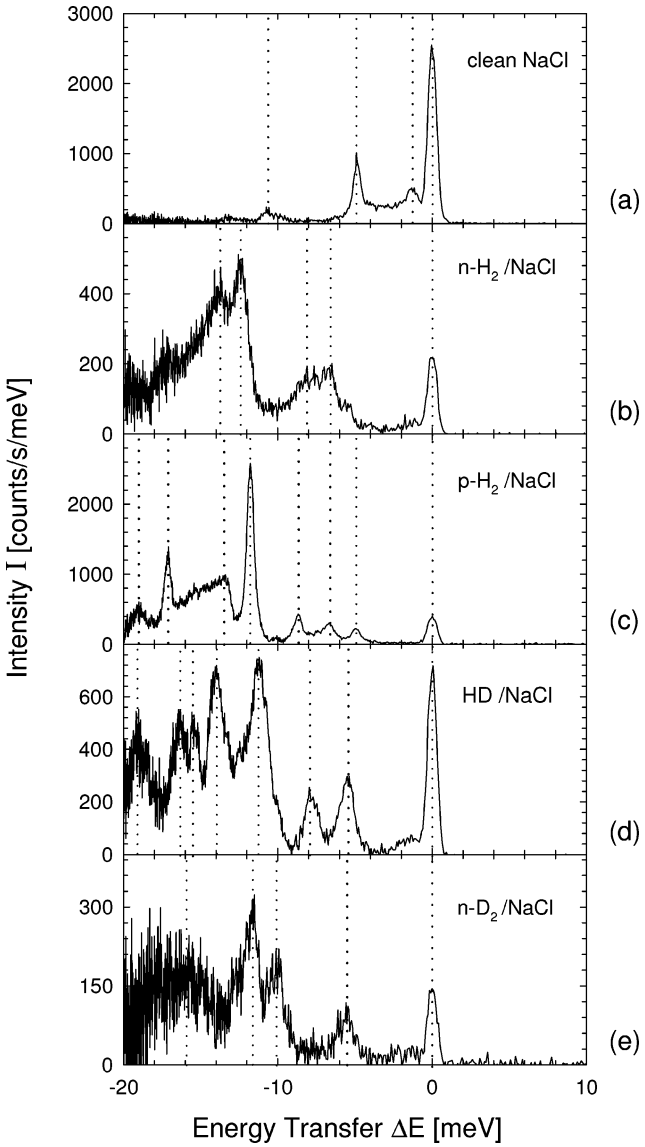

Figure 13. Comparison of (a) typical TOF spectra of the bare NaCl surface with spectra for monolayers of (b) n-H_2, (c) p-H_2, (d) HD, and (e) n-D_2. These spectra were all measured along the [110] azimuth at an incident angle of $\theta_i = 44°$, surface temperature of 8 K, and a beam energy of 26.5 meV. The gas pressures were slightly different and the same as in the corresponding spectra in Figures 5, 7, 10, and 12.

than the intermolecular distance in the hydrogen solid of 3.747 Å at zero pressure.[24]

Grunwald and Ewing[44] interpreted their infrared measurements at a lower temperature of 5.2 K in terms of two occupied neighboring adsorption sites: One above a surface cation, occupied by molecules in $j = 0$, and a second adsorption site above a surface anion, occupied only by molecules in the $j = 1$ rotational state. The occupation of these close-lying adsorption sites is sterically possible, as the height above an anion site is sufficiently greater than that above a cation because of the different ionic radii. Elsewhere, for HD/NaCl,[79] the same authors, citing calculations by Folman and Kozirovski,[80] propose that steric hindrance is also avoided by orienting the molecules at the anion sites perpendicular to the surface with the molecule 3.48 Å above the surface, which is much larger than for the parallel-oriented molecules which lie 2.47 Å above cation sites.

The surface temperature of about 8 K, at which most of the present experiments were carried out, lies between the conditions of these IR studies. The lack of any superstructure diffraction peaks along the [100] and [110] high-symmetry directions (see Figures 2 and 3) provides rather direct evidence against a structure with a symmetry different from (1×1). In the symmetries of the unit cell, however, there is no information on the coverage. The presence of only one jump in both the adsorption (Figure 1) and desorption curves is not in accord with the possible adsorption of molecules on different adsorption sites and is, therefore, not in accord with dense structures with large unit cells or even double layers. In principle, for other structures with a larger unit cell and glide planes along the high-symmetry directions, e.g., $(\sqrt{2} \times \sqrt{2})$R45°, the observed superstructure diffraction peaks along [110] and [100] would be extinguished. Thus, although the evidence is not indisputable, a structure with (1×1) symmetry and one molecule per unit

TABLE 3: Summary of the Measured Average T-Mode Energies for the Different Hydrogen Isotopomers and the Assignments Discussed Here[a]

adsorbate	mode energy (meV)	transition[b]	energy as derived from p-H_2 (meV)
p-H_2	7.0	$0 \rightarrow 1$	−
	11.8	$0 \rightarrow 2$	−
	17.2	$0 \rightarrow 3$	−
o-H_2	7.7 ± 0.5	$0 \rightarrow 1$	−
	13.2 ± 0.5	$0 \rightarrow 2$	−
HD	5.6	$0 \rightarrow 1$	4.0
	7.6	2D rotation (or n-H_2)	−
	10.9	$0 \rightarrow 2$ or 3D rotation	9.6 (for vibration)
	∼14	$0 \rightarrow 3$	14.0
	∼16	$0 \rightarrow 4$ (or $\perp$)	not available
	∼19	$0 \rightarrow 5$	not available
D_2	5.5 ± 0.7	$0 \rightarrow 1$	4.9
	10.0 ± 4.0	$0 \rightarrow 2$	8.3
	17.5 ± 1.3	$0 \rightarrow 3$	12.2

[a] Only the T-mode fundamental and anharmonic overtone assignments are listed, not multiple excitations. In the case of o-H_2, the error is estimated from the deviations between the deconvolution results of several TOF spectra; for D_2, it is estimated from the width of the TOF peaks. The assignments of the HD and D_2 spectra are deduced purely from the analogy to the p-H_2 spectra, taking into account the expected isotope shift; the resulting calculated frequencies are given. [b] All modes are assigned to the translational frustrated vibration (T mode) except where indicated otherwise

cell is highly likely to be correct, as there are no observations indicating a more complicated structure.

The conditions of the present experiments come closest to those of the study by Heidberg et al., because their 1−2 K higher temperatures compared to the 8 K used in the present experiments is expected to have less of an effect than the relatively larger decrease from 8 to the 5.2 K used by Grunwald and Ewing. Thus, the agreement of the diffraction patterns and adsorption curves with the structure proposed by Heidberg et al. is more likely. It is also quite conceivable that, at the lower temperature of 5.2 K, a second adsorption site above a surface anion can be occupied especially under the application of a higher gas pressure. In addition, in the present experiments, no phase transition was found when the temperature was raised to 12 K. This also suggests that the same phase as in the experiment by Heidberg et al. was studied.

For the adsorbate system H_2/graphite, the least dense ordered phase is a $(\sqrt{3} \times \sqrt{3})$R30° phase, which is stabilized by the strong zero-point vibration of the H_2 molecules and can be uniaxially compressed upon an increase of coverage. For the present system, we are not aware of calculations that would take into account these kind of quantum effects. From the experimental point of view, there is no evidence for any additional denser phases up to a steady-state pressure of about 1×10^{-5} mbar.[75] However, the adsorbate systems H_2/MgO[37] and H_2/LiF[81] show behavior similar to that of the graphite system. It is especially interesting to compare the adsorbate on NaCl to that on the similar alkali halide surface LiF. As the hydrogen gas pressure is increased, the H_2 adsorbate on the more compact LiF lattice shows a sequence of continuous transitions, and the corresponding structures appear to be incommensurate. This observation, i.e., the absence of a (1×1) phase on the LiF surface with smaller lattice constants, is consistent with the steric argument of Heidberg et al. in favor of the (1×1) structure on NaCl.

4.2. Assignment of the Vibrational Modes. The assignments of the observed inelastic peaks, compiled in Table 3, have been largely facilitated by comparisons of the experimental vibrational energies with the calculations reported by Briquez[82] for the vibrations of single adsorbate molecules based on a pairwise-additive potential model. To apply these results to the monolayer of the present study, it is necessary to assume decoupled Einstein oscillators. The most convincing experimental evidence for neglecting the coupling between adjacent molecules in the monolayers comes from TOF spectra of submonolayers of H_2/NaCl,[17] not reported here, which show the same vibrational energies as observed in the monolayer. This observation indicates that isolated molecules or molecules in small islands do not have frequencies differing significantly from those of a monolayer. This is also consistent with the lack of any noticeable dispersion of the measured vibrational modes as also found for rare gas monolayers on Pt(111).[77] The assumption of weak lateral coupling also seems to be reasonable in view of the small differences in the desorption energies calculated by Briquez for a complete monolayer[35] and for a single molecule. The differences of only 6 meV for p-H_2 ($j = 0$) and 7.3 meV for o-H_2 ($j = 1$, $m = \pm 1$) per molecule are only about 17% of the adsorption energies of 37 meV (p-H_2) and 40 meV (n-H_2) for a complete layer. Finally, it is noted that, in other heavier systems, for example, N_2/MgO, a frequency shift with coverage has been observed.[83]

The lack of dispersion in adsorbate modes might be due to a large corrugation of the molecule−surface potential, which traps and isolates the molecules. He atom scattering from the system H_2/MgO reveals dispersive modes.[37,84] To be able to compare these systems, eikonal calculations for the scattering of H_2 beams from NaCl and MgO have been performed, but roughly the same geometric corrugation amplitudes are found.[17]

With the above justification, the measured frequencies will be compared to single-molecule frequencies. For the fundamental parallel vibration (T mode) of isolated p-H_2 state molecules in $j = 0$ above cation sites of the NaCl(001) surface and the first two overtones, Briquez et al.[36] predict energies of 6.2 meV ($0 \rightarrow 1$), 13.0 meV ($0 \rightarrow 2$), and 20.8 meV ($0 \rightarrow 3$), whereas the perpendicular fundamental (S mode) is predicted at 18.1 meV. Because the mode measured at 7.0 meV is only 12% larger than the theoretically predicted parallel mode it can be safely assigned to the fundamental T mode. Assuming a small amount of anharmonicity, then, the two sharp peaks at −11.8 and −17.2 meV are attributed to the first and second overtones, respectively. It is somewhat unusual that the difference between the first and second energy levels is smaller than that between the second and third. This effect is found in the calculations by Heidberg et al.[35] as well and is a signature of the very steep and nearly vertical potential well on this largely corrugated surface.

The alternative interpretation of the peak at −17.2 meV in terms of the perpendicularly polarized mode as suggested by the closeness to the predicted 18.1 meV is not compelling. The intensity of the energy loss peak increases with higher parallel momentum transfer, which is considered to be the signature for a parallel-polarized mode.[85] For a perpendicular mode, the relative intensity is nearly constant with parallel momentum transfer. In the TOF spectra around $\theta_i = 44.5°$ (Figure 5), there are some indications for an additional peak at slightly higher energy transfers of about −19 meV (indicated by arrows in Figure 5), which might be due to a perpendicular vibration.

The mode at 8.5 meV is the only feature observed in the disperion curve for p-H_2/NaCl(001) that is related to the substrate phonons. It seems to orginate from an avoided crossing of the substrate Rayleigh mode and the fundamental adsorbate vibration. As known from previous He atom scattering studies

not only (anharmonic) overtones, i.e., $0 \rightarrow 2, 3, ...$, transitions, can be excited but also multiples of the fundamental.[85] Thus, the broad maximum found for p-H_2 between the peaks at -11.8 and -17.2 meV can be explained as double excitations of the low-frequency modes at around 7 and 8.5 meV. Depending on the incident angle and parallel momentum transfer the two extremal phonon transitions ($2 \times 6.7 = 13.2$ and $2 \times 8.5 = 17$ meV) or the combination ($6.7 + 8.5 = 15.2$ meV) can either singly or collectively explain the energy transfers between -14 and -16 meV. These peaks are expected to be broader than the single-phonon events, because there certainly will be some dispersion in the contributing modes. Hence, it is reasonable to assume that the resulting energy transfers are not clearly resolved and add up to produce a broad maximum. The gradual shift from about -13 to -14 meV in the position of this peak with increasing incident angle can be explained by a shift of the tranferred intensity to larger energies with increasing parallel momentum transfer.

As stated above, a completely satisfactory deconvolution of the TOF spectra of the n-H_2 adsorbate layer into its ortho and para contributions, especially at high energy transfers, is quite difficult, and therefore, only the two peaks with the lowest energy transfers of -7.7 and -13.2 meV will be discussed. Assuming that the o-H_2 peaks adjacent to the p-H_2 peaks have the same origin, then the o-H_2 peak at -7.7 and -13.2 meV (Figure 8) can be assigned to the fundamental and first overtone of the T mode, respectively. These energies lie above the theoretical predictions for the $j = 1$, $m_j = \pm 1$ state of 4.8 and 11.0 meV[82] by 38% and 17%, respectively. Compared to the same levels measured for p-H_2, they both lie nearly 10% higher in frequency. The similarity in the change in intensity with increasing incident angle to that for the p-H_2 adsorbate suggests that the same assignment is justified for both isotopomeric species.

The interpretation of the HD frequencies is less straightforward. From a comparison with the p-H_2 spectra, the peak at -5.6 meV is assigned to the fundamental vibration of the T mode, whereas the origin of the peak at -7.6 meV is not as clear. This peak lies midway between the values of -5.7 and -9.6 meV estimated from the p-H_2 T-mode peak at -7.0 and its first overtone at -11.8 meV by accounting for the increase in mass. An explanation in terms of a T mode also seems unlikely, because in contrast to all T modes observed for p-H_2 and n-H_2, its intensity does not change much over the measured range of incident angles. The -7.6 meV peak might also be due to a 2D molecular rotation on the surface,[66,86] which, for the homonuclear isotopomers, lies far too high in energy. On the surface a $0 \rightarrow 1$ rotational transition is expected to have one-half the energy of a 3D (gas phase) rotation if the rotation is fully constrained to a 2D plane,[66] because $E_{2D} = Bj^2$ instead of $E_{3D} = hBj(j + 1)$, where B is the rotational constant. Consequently, with $E(0 \rightarrow 1) = 11.06$ meV in the gas phase,[66] the 2D rotation would be expected at 5.53 meV. In view of the simplicity of the theoretical model, the difference from 7.6 meV might not be significant. For the adsorbate system H_2/Cu(510), Svensson et al.[87] indeed find both a 3D rotation on terraces and a 2D rotation on step sites. Yet another possible, but unlikely explanation for the peak at about -7.6 meV could be the presence of a small amount of o-H_2 in the HD adsorbate from the 1.8% H_2 impurity in the HD gas. The adsorption of o-H_2 in a detectable amount must be considered to be highly unlikely, however, given that the partial pressure of H_2 during the HD experiments was only 2×10^{-9} mbar and considerably lower than the pressure needed to maintain a H_2 layer. The next highest peak at -10.9 meV can tentatively be assigned to a $0 \rightarrow 2$ overtone of the parallel vibration, although it might also be due to excitation of the 3D molecular $0 \rightarrow 1$ rotation (11.06 meV) as found for the terrace sites of H_2/Cu(510).[87]

In the spectra of D_2/NaCl, the signal-to-noise ratio is much less favorable. Comparable to the trend in the series of spectra for H_2/NaCl, in Figure 12, the overall intensity maximum of the D_2 spectra shifts to larger energy transfers with increasing parallel momentum transfers. In addition, the main constituent of o-D_2 is in the $j = 0$ rotational state. Both aspects suggest an assignment in analogy to the p-H_2 adsorbate. Taking into account the isotope shift and the results from the p-H_2 spectra, the $0 \rightarrow 1$, 2, and 3 T-mode transitions are expected at 4.9, 8.3, and 12.2 meV, respectively. The first deviate $+11$ and -17% from the experimental values (Table 3), which is within the experimental errors of ± 0.7, ± 4.0, and ± 1.3 meV for the $0 \rightarrow 1$, 2, and 3 transitions, respectively. Close to the $0 \rightarrow 2$ transition there is also a peak that can be assigned to a double T-mode excitation or to an S-mode excitation. The peak at energy transfers larger than 15 meV is more difficult to assign, because the deviation from the $0 \rightarrow 3$ transition as expected from p-H_2 is more than 40%. However, the assignment to the second overtone of the T mode is supported by the pronounced gain in relative intensity in going from an incident angle of 38° to 47°.

Further support for the interpretation of the measured modes of the p-H_2 monolayer solely in terms of parallel vibrations comes from a comparison of the TOF intensities with calculations based on a semiclassical theory recently developed by Li et al.[85] For the adsorbate system CO/Cu(001), they could simulate the intensities of the parallel frustrated translational mode (T mode) with harmonic overtone excitations, a perpendicular substrate−adsorbate stretching mode (S mode) as well as a frustrated rotational mode (R mode). To assign the polarizations for the present system, three models were used in which, for simplicity, only three *independent* modes at 7, 12, and 17 meV were assumed and, moreover, the mode at 7 meV was preassigned to a T mode. The other two higher-energy modes can be either S or T modes. In model I, all modes are T-polarized. In model II, the mode at 12 meV is S-polarized, and the mode at 17 meV is T-polarized. In model III, the mode at 12 meV is T-polarized, and the mode at 17 meV is S-polarized. In applying these models, corrections were made for the following two effects, the second of which had not been accounted for in previous theories:[85,88] First, the ionization probability of the detector was made proportional to the inverse of the He atom velocity and therefore proportional to c/k_f, where c is a constant. Second, the beam density at the detector was corrected for the ratio of the angular divergences before and after the collision. The divergence of the incident and scattered He beams is given by $\Delta k_\perp/k_{f,i}$, and assuming that the velocity perpendicular to the direction of the beam is not changed during the collision the detection probability is proportional to $(\Delta k_\perp/k_i)(k_f/\Delta k_\perp) = k_f/k_i$. The product of the two correction factors, $(c/k_f)\cdot(k_f/k_i)$, results in the factor c/k_i, where c cancels out in comparing relative intensities. In Figure 14, the areas under the peaks for a typical p-H_2 TOF spectrum at $\theta_i = 44°$ are compared with the calculated probabilities for the three models. As seen in Figure 14a, model I with only T polarization gives the best agreement. In models II and III, shown in Figure 14c and d, the S-polarized peak dominates the spectrum, which is not observed experimentally. For model I, there is also an apparent discrepancy in the measured and calculated intensities of the peaks at 0 and -14 meV. To interpret this correctly, the different origins of the 0 meV peak in theory and experiment have to be

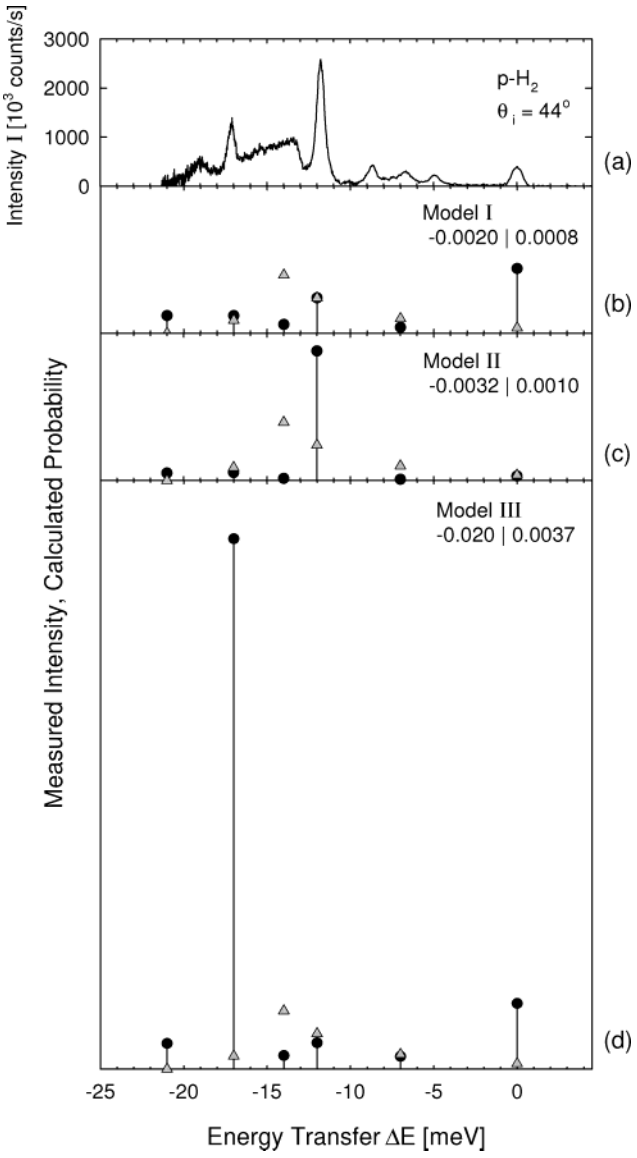

Figure 14. Comparison of the integrated intensities (gray triangles) from the experimental spectrum in a with the calculated probabilities (filled circles) with the models I, II, and III in b−d, respectively. The scale of the vertical axis is the same for cases b−d. As seen from the figures and from the average and largest deviation given in the insets, the best fit is obtained for model I based on the assumption that the modes are not S-polarized.

taken into account. From previous experience in HAS, it is known that the main contribution to the peak at 0 meV is diffuse elastic scattering from defects.[74] This effect is not included in the calculations, which attribute the peak to virtual transitions corresponding to combined creation-annihilation events, e.g., an energy loss of 7 meV plus a subsequent gain of 7 meV adding up to an overall energy loss of 0 meV. Thus, because the calculated intensity of the 0 meV peak is greater than in the experiment, it appears that the theory overestimates the annihilation probability of the −7 meV peak. Because this intensity is withdrawn from the −14 meV creation peaks, it also explains why this peak is too small compared to experiment. In addition, further model calculations for different incident angles agree qualitatively with the observed trend that the creation of higher-energy T modes becomes more pronounced at higher incident angles (parallel momentum transfers). Because of this pronounced shift in intensity from lower-energy T modes to the higher-energy T modes over a range in parallel momentum transfers that is larger than one Brillouin zone, it would be misleading to analyze the intensity of each mode separately, as reported for other systems.[89] Thus, all comparisons with the theory confirm the interpretation of the spectrum exclusively in terms of T modes.

4.3. Conflicting Evidence Regarding the Adsorption Probability of Ortho- and Para-H_2. *4.3.1. Variation of the n-H_2 Gas Pressure.* Because the external vibrations of p-H_2 and o-H_2 have slightly different frequencies, the time-of-flight spectra could be used to identify the particular hydrogen nuclear spin modification adsorbed under varying experimental conditions. The integration times for a typical TOF spectrum of about 33 min, however, puts a limit on the time resolution of the adsorption/desorption processes that is far above the expected time scale for such processes. Some information on para/ortho differences could however be obtained from the following two experiments: (i) a series of TOF spectra was measured for a sequence of increasing n-H_2 gas pressures and (ii) several TOF spectra were measured during desorption of the hydrogen layer without backfilling of the adsorbate gas.

In the first experiment, a TOF spectrum for a layer of pure p-H_2 plotted in Figure 15a is compared with three TOF spectra for increasing n-H_2 dosages of 2.5×10^{-8}, 8.7×10^{-8}, and 9.3×10^{-7} mbar (panels b−d). All other parameters were unchanged. As illustrated in Figure 8, the spectra in Figure 15b−d suggest that, with increasing n-H_2 pressure, the characteristic p-H_2 peaks become less pronounced, indicating an increase in the o-H_2 fraction. In the bottom panel (Figure 15e), the increase in the o-H_2 concentration on the surface is seen more clearly. For this plot, spectra in panels b−d were all normalized to the −11.8 meV p-H_2 peak; then, the p-H_2 spectrum in panel a was subtracted from each, and these differences are plotted. These measurements provide clear evidence that the relative fraction of o-H_2 on the surface increases with increasing n-H_2 pressure.

In attempting to explain the observed differences in the adsorption behavior of H_2 molecules in the ortho and para spin states on NaCl(001) surfaces, reference is made to an experiment by Heidberg et al.[35] They could explain the ortho-to-para ratio in the adsorbate, by taking the competition of kinetic and thermodynamic effects into account. For p-H_2, their experimental value of 31 ± 10 meV for the adsorption energy determined in this way is in reasonable agreement with their theoretical value of 34.5 meV. For o-H_2 ($j = 1$, $m_j = \pm 1$), their corresponding experimental and theoretical values of 38 ± 10 and 42.5 meV are, however, about 7 meV lower.[35] Their results also compare well with the adsorption energies measured in this work of 40 ± 5 meV for n-H_2 (which, in contrast to the values by Heidberg et al., is not for pure ortho) and 37 ± 5 meV for p-H_2; see Table 4. As an aside, it is interesting to recall that the larger adsorption energy of o-H_2 molecules in the $j = 1$, $m_j = 1$ rotational state, which dominates in the experiments, is due to the electrostatic interaction of the molecular quadrupole moment with the strong electric fields above the ionic surface.[13−15,35]

In view of the large differences in the adsorption energies, it is perhaps not surprising that, at 11 K, Heidberg et al. observed a pure o-H_2 monolayer, whereas when the layer was prepared at $T = 9$ K, both o-H_2 and p-H_2 were detected on the surface. Heidberg et al. explain this in terms of a 17-times larger sticking coefficient of p-H_2 compared to o-H_2. At $T \geq 11$ K, the initially preferably adsorbed p-H_2 molecules are replaced by the more strongly bound o-H_2 molecules, and thermodynamic equilibrium is approached.

The increase of the fraction of o-H_2 with increasing n-H_2 gas pressure, as shown in Figure 15, is in accord with this balance

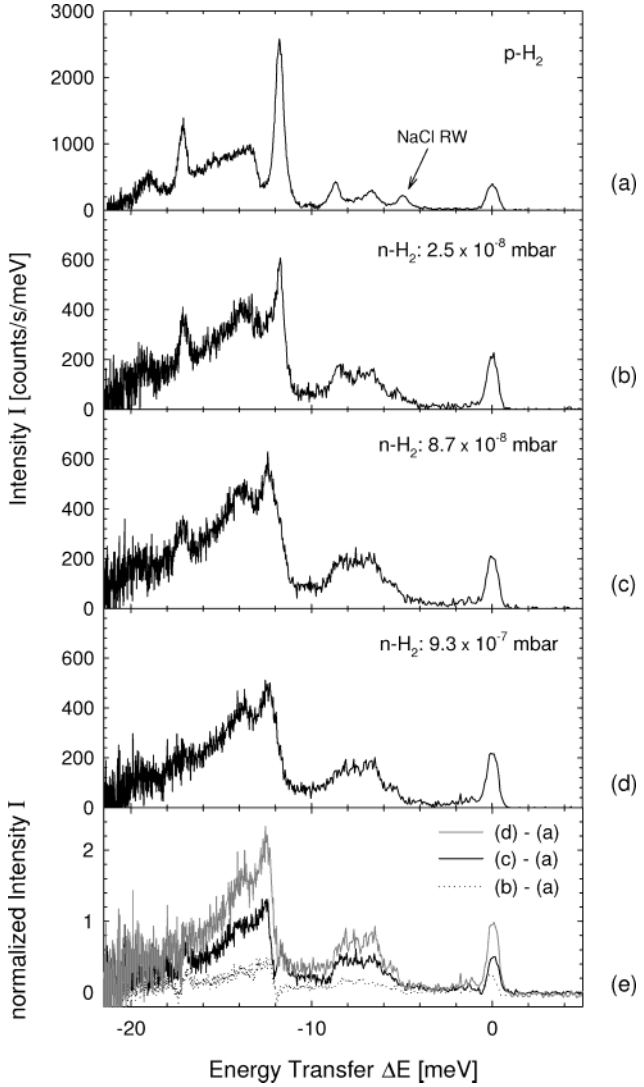

Figure 15. TOF spectra of a layer of p-H_2 under continuous exposure to (a) 1×10^{-7} mbar of p-H_2 and (b) 2.5×10^{-8}, (c) 8.7×10^{-8}, and (d) 9.3×10^{-7} mbar of n-H_2. All of these TOF spectra were taken at an incident angle of $\theta_i = 44$ °, a surface temperature of 8 K, and an incident beam energy of 26.5 meV. In panel e, the difference curves of normalized spectra b−d and spectrum a are shown.

TABLE 4: Adsorption Energies of the Different Isotopomers from Ref 35 and This Work[a]

	ref 35		
	theory	experiment	this work
para-H_2	34.5	31 ± 10	37 ± 5
ortho-H_2	42.5	38 ± 10	−
n-H_2	−	−	40 ± 5

[a] All values are in meV.

between kinetically and thermodynamically controlled adsorption. Because more collisions take place at higher gas pressure, the experiment at higher pressures should be closer to equilibrium and, therefore, should favor more o-H_2 on the surface. On the other hand, a time-dependent equilibration could not be observed in the TOF spectra even after times of about 6 h. This suggests either that equilibrium is reached almost immediately or that the approach to equilibrium takes much longer than 6 h, which would imply that the experiments are, in fact, not carried out in thermodynamic equlibrium.

4.3.2. Desorption Experiments. Figure 16 presents the data on the second (the desorption) experiment. The sequence of

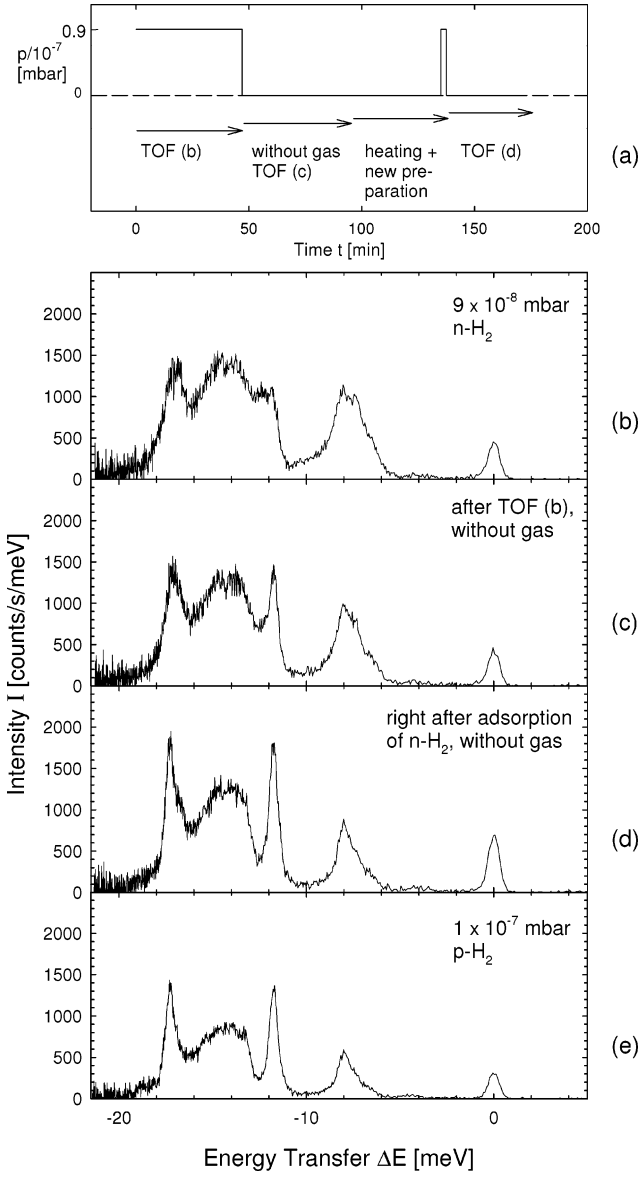

Figure 16. (a) Time scale for the adsorption/desorption experiments in panels b−d. (b) TOF spectrum at 9×10^{-8} mbar of n-H_2, (c) spectrum during desorption of the layer in b without gas dosage, and (d) TOF spectrum of H_2/NaCl(001) during desorption without further gas dosage directly after preparation of a n-H_2 layer. For reference, a spectrum of a p-H_2 layer is shown in e. All of these spectra were taken at an incident angle of $\theta_i = 47°$, a surface temperature of 8 K, and an incident beam energy of 26.5 meV.

experimental conditions and their exact time scales are indicated schematically in Figure 16a. First, under stationary conditions of a continuous dosage of 9×10^{-8} mbar of n-H_2, a TOF spectrum (panel b) was recorded. Then, the TOF spectrum in in c was measured after the gas supply had been turned off. This spectrum closely resembles the p-H_2 spectrum shown in Figure 16e, indicating that predominantly p-H_2 remains on the surface during the desorption of a layer produced by exposure to the o-H_2 in the n-H_2. Following the measurement of the TOF spectrum in c, the layer was completely desorbed, and the crystal was cleaned by heating to a temperature of about 60 K. After completion of the desorption, a TOF spectrum of the clean surface (not shown) was taken to check for impurities, which together took about 40 min. Then, a second adsorption with n-H_2 was performed, and right after completion of the layer, the gas supply was turned off, and the TOF spectrum in d was measured during the subsequent 33 min.[90] Again, the spectrum

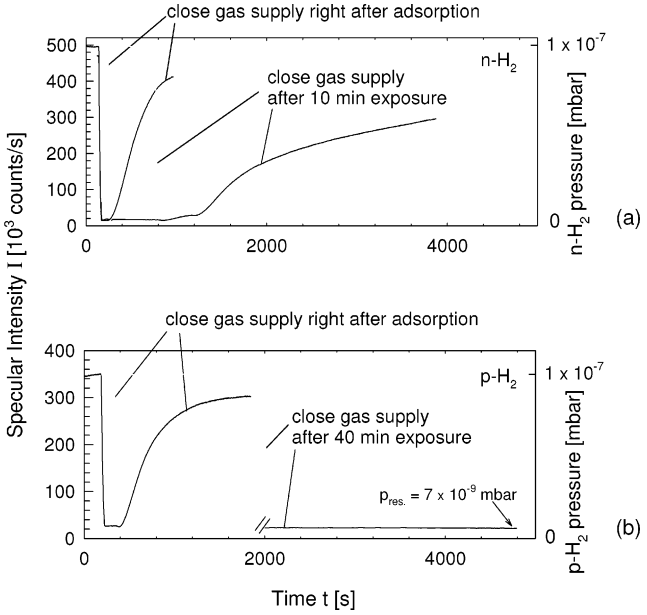

Figure 17. Desorption curves of n-H_2 and p-H_2. The solid lines show the specular intensity; the dashed lines show the gas pressure. In the case of n-H_2 (a), the n-H_2 gas supply was closed immediately after adsorption at an H_2 pressure of 1×10^{-7} mbar for the left curve and after 10 min for the right curve. In the case of p-H_2 (b), the gas supply was closed immediately for the left curve and after 40 min for the right curve. In the latter case, no desorption was detected even though the residual H_2 gas pressure was only 7×10^{-9} mbar.

reveals an enrichment of p-H_2. For comparison, these experiments were also carried out with pure p-H_2, but in confirmation of the interpretation presented here, no pressure or time dependence was found.

The effect of slow desorption of p-H_2 can be seen in the desorption curves shown in Figure 17. Closing the gas supply after adsorption, both layers of n-H_2 and p-H_2 (see a and b) desorb quickly within about 1000 s. After prolonged adsorption times, for example, 10 min for the case of n-H_2, the layer desorbs more slowly. Quite surprisingly, after 40 min of p-H_2 adsorption, the layer no longer desorbs on the time scale of the experiment. In b, the residual gas pressure, which is reached quickly after the valve is closed, is given, and at 7×10^{-9} mbar, it is more than an order of magnitude below the pressure needed for adsorption of layers of about 1×10^{-7} mbar.

In long experimental runs taking up to 3 h, the TOF spectra of n-H_2 layers that were maintained under steady-state pressures did not show any significant changes in the relative peak intensities. Therefore, a simple time dependence of the spectra that would indicate a slow approach to the thermodynamic equilibrium seems unlikely.

The results of Figures 16 and 17 appear to indicate a surface enrichment of p-H_2 at a surface temperature of 8 K, although this is in apparent contradiction to the lower adsorption energy for p-H_2 (see Table 4). Also, it cannot be simply explained by invoking only a kinetically controlled adsorption process. The TOF spectrum in Figure 16b measured during continuous exposure of the surface under 9×10^{-8} mbar of n-H_2 indicates a significant fraction of o-H_2. However, during the desorption of this layer without further gas dosage, again, mostly p-H_2 is seen (Figure 16c). The TOF spectrum measured right after adsorption of a freshly prepared layer but without further gas exposure (Figure 16d) also indicates that, during the short adsorption time, p-H_2 was predominantly adsorbed. In the thermodynamic model, more o-H_2 would be expected to be on the surface given that it is more tightly bound. In principle it is possible that during the turning off of the H_2 gas prior to the TOF spectrum, some desorption and readsorption take place as long as the H_2 pressure is not too low, as it took a few minutes to reduce the H_2 background pressure to $\leq 10^{-9}$ mbar. Then, the kinetic argument would again predict that an increased amount of p-H_2 would be found on the surface because of its larger sticking coefficient. This interpretation, however, would not agree with the dwell times of hours that were estimated by Heidberg et al.[35]

In conclusion, the present experiments show clearly that the ratio of adsorbed ortho- and para-H_2 depends on the applied H_2 gas pressure. This could be an indication that thermodynamic equilibrium is not reached. On the other hand, the observations under continuous dosage and during desorption are somewhat contradictory, which suggests that the actual behavior is more complicated than assumed in the simple models discussed here.

5. Outlook

The question, whether a 2D superfluid state can be reached in H_2 adsorbates has still not been answered experimentally. For this, the adsorbate system H_2/NaCl is perhaps not an ideal candidate system, given that the molecules are trapped in a strongly corrugated potential surface with relatively large binding energies. An upper limit for the onset temperature for superfluidity, T_c, in a 2D layer can be estimated from[70,91]

$$T_c = \frac{\rho_s \pi \hbar^2}{2m^* k_B} \tag{5}$$

where ρ_s is the 2D number density of the superfluid; m^* is the effective mass of the particle; and $\hbar$ and k_B are the Planck and Boltzmann constants, respectively. For H_2 on NaCl with $m^* =$ 2 amu and $\rho_s = \rho_{tot}$, the total density, $T_c = 2.4$ K according to eq 5. Much lower temperatures are probably required, however, as $\rho_s = 0.22\rho_{tot}$ for He films.[91] Moreover, it is highly unlikely that the layer would not be frozen at 2.4 K, given that for the similar physisorption system H_2/MgO, for example, the triple point has been determined to 11.6 K.[21] Superfluidity might be possible under special conditions, however. Gordillo and Ceperley[92] calculate that the chances of finding a superfluid transition are greatest in an incommensurate dilute hydrogen layer on a smooth substrate. For a layer of p-H_2 on a metal surface between equally spaced alkali atoms, they find the layer in a liquid state down to the transition temperature to superfluidity of $T_c = 1.2$ K.

6. Summary

The adsorption curves and the He diffraction patterns of the systems n-H_2, p-H_2, HD, and n-D_2 on NaCl all indicate a well ordered, highly corrugated (1×1) monolayer structure as first proposed by Heidberg et al.[35] on the basis of indirect infrared measurements and potential calculations.

The TOF spectra of p-H_2/NaCl reveal three sharp modes at 7.0, 11.8, and 17.2 meV and an additional broad peak between the latter two. From comparisons with potential calculations by Briquez et al.[36] and semiclassical model calculations of TOF intensities using a model by Li et al.,[85] all of the sharp peaks are assigned to a parallel frustrated translational mode (T mode) and its anharmonic overtones. After a crossing of the fundamental vibration with the NaCl Rayleigh mode, a new mode at 8.5 meV appears at the zone boundary. The broad peak is assigned to a superposition of double excitations of the T-mode vibrations.

The TOF spectra of n-H_2 reveal broad energy transfer peaks that can be explained by a superposition of o-H_2 and p-H_2 inelastic peaks. From a deconvolution of the spectra, mode energies of 7.7 meV are assigned to the fundamental o-H_2 T-mode vibrations and 13.2 meV to the first overtone. The ratio of ortho/para hydrogen is influenced by the H_2 gas pressure and probably also by kinetic effects. In experiments under continuous dosage of n-H_2 at higher gas pressures, more o-H_2 is present on the surface, consistent with a slow approach to thermodynamic equilibrium. In contrast, without a continuous dosage of H_2 gas during the desorption of both p-H_2 and n-H_2 layers, mainly p-H_2 is found on the surface.

Monolayers of HD and n-D_2 have also been investigated. Most peaks in their TOF spectra can be explained using the above arguments if the isotope mass shift for a harmonic oscillator is taken into account. In addition, a molecular rotation of the adsorbed HD molecules has possibly been excited in the He scattering experiment.

Acknowledgment. The authors thank J. R. Manson for enlightening discussions about this work and for providing us with a copy of his computer program for the calculation of TOF intensities. Finally, we are happy to have this opportunity to thank Gerhard Ertl for his continuing enthusiastic interest in our HAS experiments. In the early 1980s during a visit to his laboratory in Munich, he was probably the first colleague to call our attention to the lack of data on frustrated translation modes and the new opportunities HAS provided. The present contribution is in many respects the culmination in a long series of experiments, recently reviewed by a member of our group,[76] that prove the wisdom of his prophesy.

References and Notes

(1) Estermann, I.; Stern, O. *Z. Phys.* **1930**, *61*, 95.
(2) Frisch, R. *Z. Phys.* **1933**, *84*, 443.
(3) Stern, O. *Z. Naturwiss.* **1929**, *17*, 391.
(4) deBroglie, L. *Philos. Mag.* **1924**, *47*, 446.
(5) Rowe, R. G.; Ehrlich, G. *J. Chem. Phys.* **1975**, *63*, 4648.
(6) Rowe, R. G.; Rathburn, L.; Ehrlich, G. *Phys. Rev. Lett.* **1975**, *35*, 1104.
(7) Boato, G.; Cantini, P.; Mattera, L. *J. Chem. Phys.* **1976**, *65*, 544.
(8) Chiesa, M.; Mattera, L.; Musenich, R.; Salvo, C. *Surf. Sci.* **1985**, *151*, L145.
(9) Yu, C. F.; Whaley, B.; Hogg, C. S.; Sibener, S. J. *Phys. Rev. Lett.* **1983**, *51*, 2210.
(10) O'Keefe, D. R.; Smith, J. E.; Palmer, R. L.; Saltsburg, H. *J. Chem. Phys.* **1970**, *52*, 4447.
(11) Mattera, L. In *Atomic and Molecular Beam Methods*; Scoles, G., Ed.; Oxford University Press: Oxford, U.K., 1992; p 366 and references therein.
(12) Farias, D.; Rieder, K. H. *Rep. Prog. Phys.* **1998**, *61*, 1575 and references therein.
(13) Kroes, G. J.; Mowrey, R. C. *Chem. Phys. Lett.* **1995**, *232*, 258.
(14) Kroes, G. J.; Mowrey, R. C. *J. Chem. Phys.* **1995**, *103*, 2186.
(15) Pijper, E.; Kroes, G. J. *Phys. Rev. Lett.* **1998**, *80*, 488.
(16) Bertino, M. F.; Glebov, A. L.; Toennies, J. P.; Traeger, F.; Pijper, E.; Kroes, G. J.; Mowrey, R. C. *Phys. Rev. Lett.* **1998**, *81*, 5608.
(17) Traeger, F. Ph.D. Thesis, Max-Planck-Institut für Strömungsforschung and Universität Göttingen, Göttingen, Germany, 2001.
(18) It is interesting to note that the underlying differences in the interaction of the two isotopes had already been anticipated in 1978 in the course of theoretical studies of adsorbate films of H_2.[19]
(19) Gready, J. E.; Bacskay, G. B.; Hush, N. S. *J. Chem. Soc., Faraday Trans. 2* **1978**, *74*, 1430.
(20) Degenhardt, D.; Lauter, H. J.; Haensel, R. *Jpn. J. Appl. Phys.* **1987**, *26*, 341.
(21) Vilches, O. E. *J. Low Temp. Phys.* **1992**, *89*, 267.
(22) Vilches, O. E.; Liu, F. C.; Kingsbury, D. L.; Ma, J.; Bienfait, M.; Suzanne, J.; Gay, J. M.; Maruyama, M.; Zeppenfeld, P.; Degenhardt, D.; Lauter, H. J.; Rieutord, F.; Coddens, G. In *Excitations in Two-Dimensional Quantum Fluids and Three-Dimensional Quantum Fluids*; Wyatt, A. G. F., Lauter, H. J., Eds.; Plenum Press: New York, 1991; p 477 and references therein.
(23) Maruyama, M.; Bienfait, M.; Liu, F.-C.; Vilches, O. E.; Rieutord, F. *Surf. Sci.* **1993**, *283*, 333.
(24) Ma, J.; Kingsbury, D. L.; Liu, F.-C.; Vilches, O. E. *Phys. Rev. Lett.* **1988**, *61*, 2348.
(25) Jeong, E.-C.; Ouyang, B.; Norberg, R. E.; Fedders, P. A.; Conradi, M. S. *Phys. Rev. Lett.* **1992**, *69*, 2983.
(26) Wiechert, H. In *Physics of the Covered Solid*; Landolt Börnstein, New Series III, 42A3; Springer: Berlin, 2003; p 166.
(27) Cui, J.; Fain, S. C., Jr.; Freimuth, H.; Wiechert, H.; Schildberg, H. P.; Lauter, H. J. *Phys. Rev. Lett.* **1988**, *60*, 1848.
(28) Freimuth, H.; Wiechert, H.; Schildberg, H. P.; Lauter, H. J. *Phys. Rev. B* **1990**, *42*, 587.
(29) Cui, J.; Fain, S. C., Jr. *Phys. Rev. B* **1989**, *39*, 8628.
(30) Kubik, P. R.; Hardy, W. N.; Glattli, H. *Can. J. Phys.* **1985**, *63*, 605.
(31) Harris, A. B.; Berlinsky, A. J. *Can. J. Phys.* **1979**, *57*, 1852.
(32) Nielsen, M.; McTague, J. P.; Ellenson, W. *J. Phys. (Paris)* **1977**, *38*, C4−10.
(33) Wiechert, H. In *Excitations in Two-Dimensional Quantum Fluids and Three-Dimensional Quantum Fluids*; Wyatt, A. G. F., Lauter, H. J., Eds.; Plenum Press: New York, 1991; p 499 and references therein.
(34) Schildberg, H. P.; Lauter, H. J.; Freimuth, H.; Wiechert, H.; Haensel, R. *Jpn. J. Appl. Phys.* **1987**, *26*, 343.
(35) Heidberg, J.; Vossberg, A.; Hustedt, M.; Thomas, M.; Briquez, S.; Picaud, S.; Girardet, C. *J. Chem. Phys.* **1999**, *110*, 2566.
(36) Briquez, S.; Picaud, S.; Girardet, C.; Hoang, P. N. M.; Heidberg, J.; Vossberg, A. *J. Chem. Phys.* **1998**, *109*, 6435.
(37) Skofronick, J. G.; Toennies, J. P.; Traeger, F.; Weiss, H. *Phys. Rev. B* **2003**, *67*, 035413.
(38) Ben Ephraim, A.; Folman, M. *J. Chem. Soc., Faraday Trans. 2* **1976**, *72*, 671.
(39) Day, D. J.; Ewing, G. E. *J. Chem. Phys.* **1993**, *98*, 5050.
(40) Day, D. J.; Ewing, G. E. *J. Chem. Phys.* **1994**, *100*, 1.
(41) Heidberg, J.; Dierkes, W.; Schönekäs, O.; Schwarte, R. *Ber. Bunsen-Ges. Phys. Chem.* **1994**, *98*, 131.
(42) Heidberg, J.; Gushanskaya, N. Y.; Schönekäs, O.; Schwarte, R. *Surf. Sci.* **1995**, *331*−*333*, 1473.
(43) Heidberg, J.; Gushanskaya, N. Y.; Schönekäs, O.; Schwarte, R. *Microchim. Acta* **1997**, *14*, 643.
(44) Grunwald, M.; Ewing, G. E. *J. Chem. Phys.* **1998**, *109*, 4990.
(45) Skofronick, J. G.; Toennies, J. P.; Traeger, F., to be published.
(46) Brusdeylins, G.; Doak, R. B.; Toennies, J. P. *Phys. Rev. B* **1983**, *27*, 3662.
(47) Toennies, J. P.; Winkelmann, K. *J. Chem. Phys.* **1977**, *66*, 3965.
(48) Toennies, J. P.; Vollmer, R. *Phys. Rev. B* **1991**, *44*, 9833.
(49) For the studies reported here, a NaCl crystal was mounted onto a low-temperature manipulator, which is described in more detail in a previous publication on H_2/MgO.[37] A somewhat different sample holder than the one described there was used. The one used here consisted of a copper block with a rectangular recess into which the sample was pressed. For measurements along the [110] direction, the sample had to be mechanically cut to fit into this recess, which led to a slight misalignment of the crystal direction, as can be seen from the slightly asymmetric intensity distribution between the ($\pm m$, 0) Bragg peaks of the angular distributions. Fortunately, the measurement of inelastic time-of-flight spectra, which was the main part of this study, is not sensitive to these small deviations in alignment.
(50) Scientific Instruments Inc., 4400 W. Tiffany Drive, Mangonia Park, West Palm Beach, FL 33407.
(51) *Gmelins Handbuch der Anorganischen Chemie, Natrium*, 8th ed.;Verlag Chemie: Weinheim, Germany, 1973; Vol. 21, Supplemental Vol. 6, pp 23, 48, and 100.
(52) *Handbook of Chemistry and Physics*, 62th ed.; Weast, R. C., Ed.; CRC Press: Boca Raton, FL, 1985.
(53) Glebov, A. L.; Toennies, J. P.; Weiss, H. *Surf. Sci.* **1996**, *351*, 200.
(54) Ioannotta, L.; Scoles, G.; Valbusa, U. *Surf. Sci.* **1985**, *161*, 411.
(55) ξ is the geometric corrugation amplitude of the He−NaCl interaction potential, which was obtained by an analysis of He diffraction intensities in terms of the eikonal approximation.
(56) Chen, T. S.; deWette, F. W.; Aldredge, G. P. *Phys. Rev. B* **1977**, *15*, 1167.
(57) Benedek, G.; Miglio, L. In *Ab Initio Calculation of Phonon Spectra*; Devreese, J. T., van Doren, V. E., von Camp, P. E., Eds.; Plenum Press: New York, 1982; p 215.
(58) Benedek, G.; Brusdeylins, G.; Doak, R. B.; Skofronick, J. G.; Toennies, J. P. *Phys. Rev. B* **1983**, *38*, 2104.
(59) Safron, S. A.; Brug, W. P.; Chern, G.; Duan, J.; Skofronick, J. G. *Vac. Sci. Technol.* **1990**, *A8*, 2627; **1991**, *A9*, 1657.
(60) Glebov, A.; Silvestri, W.; Toennies, J. P.; Benedek, G.; Skofronick, J. G. *Phys. Rev.* **1996**, *B 54*, 17866.
(61) Glebov, A. L.; Toennies, J. P.; Skofronick, J. G.; Manson, J. R. *Phys. Rev. B* **1998**, *58*, 10012.
(62) Messer Griesheim GmbH, Fütingsweg 34, 47805 Krefeld, Germany.
(63) Campro Scientific, Grosser Wall 77, 46422 Emmerich, Germany.

(64) Rox, T. Ph.D. Thesis, Max-Planck-Institut für Strömungsforschung and Universität Göttingen, Göttingen, Germany, 1992.
(65) Josefowski, L.; Ottinger, Ch.; Rox, T. *Chem. Phys. Lett.* 1992, *190*, 323.
(66) Souers, P. C. *Hydrogen Properties for Fusion Energy*; University of California Press: Berkeley, CA, 1986.
(67) Toennies, J. P. In *Surface Phonons*; Kress, W., deWette, F. W., Eds.; Springer Series in Surface Sciences 21; Springer: Berlin, 1991, pp 111−166.
(68) Poelsema, B.; Comsa, G. *Scattering of Thermal Energy Atoms from Disordered Surfaces*, Springer Tracts in Modern Physics; Springer: Berlin, 1989.
(69) Lange, G.; Schmicker, D.; Toennies, J. P.; Vollmer, R.; Weiss, H. *J. Chem. Phys.* **1995**, *103*, 2308.
(70) Bruch, L. W.; Cole, M. W.; Zaremba, E. *Physical Adsorption: Forces and Phenomena*; International Series of Monographs on Chemistry 32; Clarendon Press: Oxford, U.K., 1997; pp 108 p 138.
(71) Ferry, D.; Glebov, A.; Senz, V.; Suzanne, J.; Toennies, J. P.; Weiss, H. *J. Chem. Phys.* **1996**, *105*, 1697.
(72) Bruch, L. W.; Glebov, A. L.; Toennies, J. P.; Weiss, H. *J. Chem. Phys.* **1995**, *103*, 5109.
(73) Picaud, S.; Girardet, C.; Glebov, A.; Toennies, J. P.; Dohrmann, J.; Weiss, H. *J. Chem. Phys.* **1997**, *106*, 5271.
(74) Lahee, A. M.; Manson, J. R.; Toennies, J. P.; Wöll, Ch. *J. Chem. Phys.* **1987**, *86*, 7194.
(75) Only one feature in the angular distribution is still puzzling. At very low incident energies of about 10−15 meV on very pure monolayers, a small satellite peak about 0.35 $Å^{-1}$ apart from the specular peak is found. We have not interpeted it as a diffraction peak of an incommensurate superstructure, given that it is not repeated at other positions in the Brillouin zone; it is not visible at higher incident energies; and its intensity is only about 0.05−0.3% of the specular peak intensity, which is in the range of selective adsorption resonances on the clean NaCl surface. In addition, it does not change with increasing H_2 steady-state pressure. Conceivably this could also be consistent with an explanation in terms of selective adsorption.
(76) Graham, A. P. *Surf. Sci. Rep.* **2003**, *49*, 115.
(77) Bruch, L. W.; Graham, A. P.; Toennies, J. P. *J. Chem. Phys.* **2000**, *112*, 3314.
(78) The better quality of the [110] spectra might have another trivial reason. During the experiments along [100], the H_2 gas was not quite as pure as in the subsequent experiments along [110], and hence, in the [100] experiment, the measuring times were limited by the slow contamination of the layer due to adsorption of residual gases such as water, CO, and N_2. However, a better quality of the TOF spectra along the [110] azimuth was also observed for H_2/MgO as well. In this case, the experimental conditions were comparable for the measurements along both directions,[37] so this explanation seems less likely.
(79) Day, D. J.; Ewing, G. E. *J. Chem. Phys.* **1994**, *100*, 8432.
(80) Folman, M.; Kozirovski, Y. *J. Colloid Interface Sci.* **1972**, *38*, 51.
(81) Toennies, J. P.; Traeger, F.; Weiss, H., to be published.
(82) Briquez, S. Ph.D. Thesis, Université de Franche-Comté, Besançon, France, 1997.
(83) Jack, D. B.; Sallabi, A.; Skofronick, J. G.; Toennies, J. P.; Traeger, F.; Weiss, H., to be published.
(84) Bruch, L. W. *Phys. Rev. B* **2003**, *68*, 235420.
(85) Li, Mubing; Manson, J. R.; Graham, A. P. *Phys. Rev. B* **2001**, *63*, 155410.
(86) Gadzuk, J. W.; Landmann, U.; Kuster, E. J.; Cleveland, C. L.; Barnett, R. N. *Phys. Rev. Lett.* **1982**, *49*, 462.
(87) Svensson, K.; Bengtson, L.; Bellman, J.; Hassel, M.; Persson, M.; Andersson, S. *Phys. Rev. Lett.* **1999**, *83*, 124.
(88) Manson, J. R. Clemson University. Private communication, 1999.
(89) Bortolani, V.; Franchini, A.; Nizzoli, F.; Santoro, G. *Phys. Rev. Lett.* **1984**, *52*, 429.
(90) Complete desorption without heating would have taken 50−60 min after the gas pressure had immediately fallen to less than 10% of the dosage pressure, which is significantly longer than the 35-min integration time of the TOF spectrum. Therefore, no significant influence of the TOF integration time was found.
(91) Kosterlitz, J. M.; Thouless, D. J. *J. Phys. C: Solid State Phys.* **1973**, *6*, 1181.
(92) Gordillo, M. C.; Ceperley, D. M. *Phys. Rev. Lett.* **1997**, *79*, 3010.